B E R I C H T E

aus dem

INSTITUT FÜR MEERESKUNDE

an der

CHRISTIAN-ALBRECHTS-UNIVERSITÄT · KIEL

Nr. 25

Topographic and Baroclinic Circulations In The Southwest Baltic

DOI 10.3289/IFM_BER_25

by

T. J. SIMONS

1976

Topographic and Baroclinic Circulations in the Southwest Baltic

T. J. Simons

Institut für Meereskunde, Kiel*

Abstract

Wind-driven circulations in the southwest Baltic are analyzed with reference to the combined effects of topography and stratification. Numerical results from a multi-layer nested model are compared with observations taken during the spring of 1975. It appears that the bathymetry and stratification of the southwest Baltic lead to substantial coupling of topographic and baroclinic effects.

---

*On leave from the Canada Centre for Inland Waters, Burlington, Ont.

1. Introduction

The circulation of shallow, stratified seas is to a large extent controled by topography and baroclinicity. These effects are of particular importance for the southwest Baltic with its irregular topography and large density gradients. Intrusion of saline water from the North Sea leads to a permanent stratification upon which seasonal temperature variations are superposed. A shallow ridge separates the southwest basin from the open Baltic and tends to prevent exchanges of bottom water. From a dynamical viewpoint, one of the most interesting aspects of this basin is that large depth variations occur at the level of maximum stratification, thus leading to considerable coupling of topographic and baroclinic effects.

Theoretical studies have clarified the role of topography and stratification in the circulation of oceans and atmosphere. Important tools in this effort were the concept of potential vorticity in the absence of stratification and the separation of barotropic and baroclinic modes in the absence of topography. Recent studies of coastal trapped waves have also considered the combined effects of bottom slope and baroclinicity. Like previous theories on the coupling of surface and internal waves, such studies are based on two-layer models with depth variations restricted to the lower layer, such that the equations can be linearized with respect to layer depths. Numerical models permit a quantitative evaluation of the combined effects of complicated topography and stratification encountered in natural basins. This coupling

leads to essentially two results. In the first place baroclinic motions can be excited by barotropic currents crossing depth contours, in contrast to the separable baroclinic motions originating from internal velocity variations such as Ekman currents. In the second place, vertically integrated density anomalies contribute to the potential vorticity balance in the presence of depth variations.

The present study deals with wind-driven circulations in the southwest Baltic, particularly with regard to the effects mentioned above. Numerical techniques are used to simulate currents and density variations for realistic wind forcing and the results are verified by recourse to the "Baltic 75" measurement program. This program was carried out during the spring of 1975 and concentrated on the area north and east of the island Bornholm in the southwest Baltic. Currents and temperatures were recorded continuously at depths of 15, 25, 35, 55 and 65 m in a total of about 20 locations. Additional data were collected by ship cruises, meteorological observations, and mixing experiments. A summary of this experiment has been presented by Keunecke et al (1975).

This report starts with a discussion of the dynamics of the system and the relevant equations, followed by a description of the numerical model. Next, barotropic and baroclinic circulations are considered in the context of idealized forcing conditions and the effects of topography, stratification, friction and boundary conditions are evaluated. Finally, an attempt is made to reproduce the observed circulation in the early part of May, 1975.

2. Dynamical Model Equations

The mathematical framework of the model is similar to typical oceanographic models. The hydrostatic assumption is used together with the Boussinesq approximation, and free convection is simulated by instantaneous adjustment to neutral stability conditions. Sub-grid-scale motions and mixing processes are represented by conventional eddy diffusion parameters. All time variations are described by the general conservation equation

$$(1) \qquad \frac{\partial \phi}{\partial t} + \nabla \cdot [\phi \underset{\sim}{v} + \underset{\sim}{\Gamma}(\phi)] + \frac{\partial}{\partial z} [\phi w + \gamma(\phi)] = S(\phi)$$

where ϕ is an arbitrary scalar function, t is time, ∇ is the horizontal gradient operator, z is the vertical coordinate, $\underset{\sim}{v}$ the horizontal velocity vector, w the vertical velocity component, $\underset{\sim}{\Gamma}$ the horizontal diffusive flux vector, γ the vertical flux component , and S is the net source per unit volume. For temperature and salinity predictions the source term is set equal to zero, but surface and lateral fluxes can be included through the appropriate boundary conditions. For the velocity components u, v, along the horizontal coordinates x, y, the source terms are

$$(2) \qquad S(u) = fv - \frac{\partial}{\partial x}(P + Q); \qquad S(v) = -fu - \frac{\partial}{\partial y}(P + Q)$$

where f denotes the Coriolis parameter and P and Q represent the barotropic and baroclinic pressure contributions defined

as follows

$$(3) \qquad P = g\zeta + p_s/\rho_o \qquad\qquad Q = g \int_z^\zeta \frac{\Delta\rho}{\rho_o}\, dz.$$

where ζ denotes the free surface elevation, p_s is the atmospheric pressure at the air-sea interface, ρ_o is the mean water density, $\Delta\rho$ is the density anomaly, and g is the earth's gravitational acceleration. The density anomaly is related to temperature and salinity by an equation of state or, in the absence of external sources, can be predicted immediately from (1).

The vertical velocity and the surface elevation are related to the horizontal velocities by the continuity equation

$$(4) \qquad \frac{\partial u}{\partial x} + \frac{\partial v}{\partial y} + \frac{\partial w}{\partial z} = 0$$

together with the lower boundary condition that the flow normal to the bottom be zero. At the lateral boundaries the normal component of the flow must vanish, whereas the tangential component may be nonzero as will be discussed later. Momentum fluxes at top and bottom of the model must satisfy the conditions

$$(5) \qquad \rho\gamma(u,v)_s = -\underset{\sim}{\tau}_s \qquad\qquad \rho\gamma(u,v)_b = -\underset{\sim}{\tau}_b$$

where the wind stress $\underset{\sim}{\tau}_s$ and the bottom friction $\underset{\sim}{\tau}_b$ are related to wind and bottom currents, respectively, by the usual quadratic stress laws.

The theory of large-scale circulation in the sea is largely based on the assumption that advection and horizontal fluxes of momentum are small compared to other contributions to the momentum balance. The same will be done in this study. The equations of motion then reduce to the simple form

$$(6) \qquad \frac{\partial}{\partial t}(u,v) = S(u,v) - \frac{\partial}{\partial z}\gamma(u,v)$$

where the vertical fluxes will be taken to be proportional to vertical shears in accordance with the conventional gradient hypothesis. It is of some interest to briefly summarize how the solutions of (6) are affected by baroclinicity and topography. With these solutions in mind it will then be easy to subsequently analyze the numerical results and evaluate the contributions of the separate effects and their coupling.

For a linear two-layer model with constant ratio of larger depths Charney (1955) has presented a formal separation of barotropic and baroclinic flow components. In first approximation the barotropic component consists of the vertically integrated water transport together with a linear combination of free surface and interface elevations, whereas the baroclinic component is approximated by the vertical shear of the current together with the interface elevation. The barotropic and baroclinic system of variables are each governed

by the familiar shallow water equations but in the baroclinic system the wave speed is reduced by the so-called equivalent depth and the wind stress is multiplied by the ratio of lower layer depth to total depth. It follows then immediately that the internal radius of deformation is much smaller than its external equivalent and that the wind-induced interface displacement tends to be small if the lower layer is shallower than the upper one. These basic properties of the baroclinic system are vividly demonstrated by the channel solutions of Csanady (1973).

As long as the barotropic flow is parallel to the bottom contours, its effect on the baroclinic component remains essentially negligible also in the presence of depth variations. Thus vertical displacements of isotherms are related to wind-induced internal velocity distributions rather than vertical-mean flow. Again, since maximum vertical velocities occur at the bottom of the surface wind drift layer, it will be relatively difficult to excite an interface which is located far below this level. Furthermore, the bottom slope tends to broaden the nearshore zone of wind-induced vertical motions with a corresponding decrease of the interface displacements near the lateral walls. The situation is quite different, however, if the barotropic flow crosses the depth contours. The associated divergence of the vertical-mean flow leads to vertical motions which increase towards the bottom, thus presenting a very effective mechanism for generating baroclinic response, even for a very deep interface. The interesting question is to what extent this effect can occur in a basin such as the southwest Baltic in view of the well-known fact that the barotropic circulation tends to follow the depth

contours very closely.

Another aspect of the coupling of barotropic and baroclinic effects can be illustrated by considering the vorticity of the vertically integrated transport. Denoting the latter by Ω, and neglecting variations of Coriolis parameter and surface elevation, one obtains from equs. (2) through (6) the transport vorticity equation

$$(7) \qquad \frac{\partial \Omega}{\partial t} = - J(h,P) - J(h,Q_b) + \frac{1}{\rho} \text{ curl } (\underset{\sim}{\tau}_s - \underset{\sim}{\tau}_b)$$

where J denotes the Jacobian operator, h is the water depth, and Q_b is the baroclinic pressure component evaluated at the bottom. It follows immediately from (7) that bottom topography does not affect the vorticity balance if pressure gradients due to surface slope and stratification compensate at the bottom (Welander, 1959). In practice, however, this may be only partly true and Holland (1973) has shown that topography combined with baroclinicity leads to enhanced western boundary transport in a wind-driven ocean model.

Perhaps more appropriate in the present context is the vorticity of the vertically-averaged flow, say ω , which is related to the transport vorticity as $\Omega = \omega h + \bar{v}\, \partial h/\partial x - \bar{u}\, \partial h/\partial y$, where the bar indicates a vertical average from the bottom to the surface.

The equation for this mean-flow vorticity reads

$$(8) \quad \frac{\partial \omega}{\partial t} = \frac{f}{h} \underset{\sim}{\bar{v}} \cdot \nabla h - \frac{\partial}{\partial x} \left(\frac{\overline{\partial Q}}{\partial y}\right) + \frac{\partial}{\partial y} \left(\frac{\overline{\partial Q}}{\partial x}\right) + \text{curl } \left(\frac{\underset{\sim}{\tau}_s - \underset{\sim}{\tau}_b}{\rho h}\right)$$

In this form, the vorticity balance has been discussed by Groen and Groves (1962) with particular reference to the fact that wind stress and bottom slope combine to generate mean-flow vorticity even if the wind is constant in space. It is also apparent that the Coriolis effect enters only where the mean flow crosses the depth contours and, similarly, baroclinic effects depend on the orientation of density anomalies relative to the bottom topography. For the special case of a closed channel, Bennett (1973) derived the interesting result that a wind blowing along the depth contours tends to generate currents in the same direction as the wind in shallow water but in opposite direction for depths larger than the mean for the cross-section. The importance of this mechanism with regard to circulations of shallow basins was emphasized by Rao and Murty (1970), and it will be vividly demonstrated by the subsequent computations for the southwest Baltic.

3. Numerical Model

Numerical simulation of water levels was pioneered many years ago by Hansen (1956) and such models have since been verified by numerous storm surge predictions. In recent years considerable advances have also been made in three-dimensional models of seas and oceans by borrowing the techniques of numerical weather prediction (see, e.g. Bryan, 1969; Reid, 1975; National Academy of Sciences, 1975). Verification of the latter models has so far been quite limited because of the formidable cost of any observational program suitable for this purpose. On the other hand, it is clear that a deterministic simulation of water motions must, in practice, be restricted to a finite range of scales with the remainder represented in the form of stresses and diffusion coefficients. It is essential that such model parameters be evaluated by combining models and observations.

The Baltic '75 field experiment covers only a small part of the western Baltic and it was visualized from the outset that a nested system of models should be considered. Nested grid systems or telescopic grids, consisting of fine-mesh domains embedded in larger coarse-mesh domains, are well known from the meteorological literature. The simplest approach is to first calculate the solution for the whole domain with the coarse mesh and then to use this solution only to specify the boundary conditions for the fine-mesh area. Suitable boundary conditions for limited-area integration of the general shallow water equations have been discussed by Elvius and Sundstrom (1973) and Chen and Miyakoda (1974). A more complete formulation of a nested model allows for a full interaction between the different grids, including feed-back from the small-scale solution into the outer area (see, e.g., Phillips and Shukla, 1973). In the present case

our interest is essentially limited to the fine-mesh solution and hence it is not necessary to employ an interactive nested model.

In this study a high-resolution model of the southwest Baltic is combined with a low-resolution model of the whole Baltic, in such a fashion that the latter supplies the boundary conditions for the former. In contrast to the fine-mesh model, however, the coarse-mesh model is homogeneous and the boundary conditions thus obtained are restricted to the normal component of the vertically-integrated water transport. Inspection of eqs. (2) through (6) shows that the vertical distribution of currents at the border can then be computed immediately if only the density gradients normal to the border are specified. It will be subsequently shown that, in the present case, the stratification is concentrated around a depth of 60m. The fine-mesh area has been taken large enough to fully enclose that part of the western Baltic which is deeper than 60 m. Consequently, the density gradients normal to the open boundaries may be expected to be negligible and they are taken to be zero.

The coarse-mesh grid covers the whole Baltic with a mesh size of 20 km. The fine-mesh model covers the southwest Baltic with a mesh size of 5 km. The area of the fine mesh is indicated by shading in Figure 1. The three-dimensional stratified model is confined to the area shown by dark shading; the light shading indicates a 5-km homogeneous model covering the shallow extreme western part of the Baltic. The stratified model has a vertical resolution of 4 layers concentrated

around the level of maximum stratification. Alternatively, the stratified model can have a horizontal grid spacing of 10 km and a vertical resolution of 9 layers with uniform layer depths from top to bottom. The bottom topography for the area covered by the stratified models is shown in Figure 2. Also shown are the positions of the moored instruments during Baltic '75 which are used for verification.

The vertical structure of the multi-layered model consists of a system of fixed permeable levels rather than moving material interfaces. This procedure appears most convenient for dealing with variable stratification and topography combined with baroclinicity. In the horizontal, the variables are staggered to form a lattice structure (Platzman , 1963). In a horizontal plane, the free surface, the vertical velocity, and the density are located at the center of squares, at the sides of which the velocity components are defined. Along the vertical coordinate, density and currents are defined as layer averages, whereas vertical velocities, stresses, and vertical fluxes are specified at levels separating layers. Nearly all computations were performed on a single lattice such that the two horizontal velocity components are defined at different points. For comparison, some solutions were obtained for a double-lattice grid. In the first case, only the normal component was set equal to zero at the shores, in the second case both velocity components go to zero there. The main disadvantage of a double-lattice model is its tendency to produce grid dispersion, whereas a single-lattice model permits spurious inertial frequencies as a result of spatial averaging of the Coriolis term. For instance, the equations for pure inertial motions on a staggered grid

between two parallel walls permit oscillations with frequencies $\sigma_n^2 = .5\, f^2 [1 + \cos n\pi/(N+1)]$, where N is the number of gridpoints across the channel and n ranges from 1 to N. For high resolutions the eigen frequencies combine to approach the true inertial oscillation but for low resolutions the error is substantial.

Central differences in time are employed for pressure-divergence terms and forward differences for friction-diffusion terms and all time-extrapolations are carried out by explicit methods. Since the free gravity wave imposes a very small computational time step, the external and internal modes of the model are treated separately. Thus the system of layer equations is transformed into one equation for the vertically-averaged flow and a set of equations for the current shears between adjacent layers. The time step for the internal motions is taken to be 15 min. Nonlinear advection terms are treated by a two-step method similar to the Lax-Wendroff scheme. It is verified that the numerical method conserves the volume integral of the predicted variable together with the integrated value of its square.

In principle, the solutions were obtained without allowing for advection or horizontal diffusion of momentum. Experiments with diffusion coefficients of the order of $10^6 cm^2/s$ indicated that their effects were small, even though this value is larger than those derived from observations by Schott et al (1976). Horizontal and vertical diffusion of mass was neglected in order not to obscure the transport by currents. Vertical eddy viscosity was varied from 50-100 cm^2/s at the surface to zero at the level of maximum density gradients. The wind stress coefficient was taken to be $1.6\ 10^{-3}$ and the bottom stress coefficient was set at $2.5\ 10^{-3}$. A further discussion of the model may be found in the paper by Simons (1974).

4. Barotropic Model Solutions

A number of experiments were carried out to investigate the character of the water circulations in the southwest Baltic for idealized wind forcing. An analysis was made of the effects of friction, boundary conditions, topography, and baroclinicity. This section deals with barotropic solutions; baroclinic effects are discussed in the next section. A vertically-integrated model with a grid spacing of 5 km was used for the shaded area of Figure 1. The boundary conditions at the open eastern border were obtained from a 20-km model of the whole Baltic. Inflow or outflow at the western end were specified in accordance with observations.

The barotropic circulation can be looked upon as a superposition of the divergent flow field associated with free surface displacements, the vorticity field generated by the interaction of wind and bottom topography, and the hydraulic flow through the western border of the Baltic. Whereas the divergent flow is strongly affected by the boundaries, the vorticity field is essentially locally generated. The latter is the predominant barotropic flow component in a basin with the topography of the southwest Baltic (Figure 2) and therefore the effects of the boundaries can be expected to be limited.

The divergent flow component can be largely eliminated if the forcing is gradually increased over a period of time comparable to the principal surface modes of the Baltic, that is, of the order of one day (Krauss and Magaard, 1962). Thus, in order to illustrate topographic effects, a series of experiments is carried out whereby the wind stress increases linearly from zero to 1 dyne/cm^2 during the first day and then remains constant. The resulting vertically-averaged currents,

averaged over the third day, are shown in Figures 3 and 4 for wind from the north and the east, respectively. In these figures, a vector equal to the grid mesh represents a velocity of 20 cm/s. Inspection of the flow patterns shows immediately that shallow water tends to run in the direction of the wind with deep water returning against the wind, as discussed below eq. (8).

For the above computations the fine-mesh model was connected with a coarse-mesh model of the open Baltic, but the western boundary was closed. It is known, however, that wind-induced water set-up in the western Baltic leads to strong outflow through the Danish Belts and vice versa. For the Baltic '75 period outflow data are available for the Fehmarn Belt and Øre Sund (Figure 1) from the Danish Belt Project (see, e.g. Jacobsen, 1976).

For a NE storm in early May, 1975, with sustained wind speeds close to 10 m/s, the average outflow through the west end of the Baltic was calculated to be about 10^5 m^3/s. The corresponding change of water level averaged over the whole Baltic would be about 2 cm/day, which was confirmed by verification of water level predictions by Kielmann (1976).

Although the outflow is intimately connected with the wind-induced water levels, including short-period surface oscillations, it is useful to compute the associated flow pattern in the southwest Baltic in the absence of wind. To the extent that the large-scale currents can be simulated by linear models, the total solution is simply a superposition of the wind-driven solution with closed borders (Figures 3 and 4) and

the hydraulic solution for a given outflow. Figure 5 shows the computed flow pattern after 3 days of outflow of the above magnitude. In accordance with the observations, 70% of the flow was assumed to take place through the Fehmarn Belt, the remainder through the Sund. It is of some interest to determine what proportion of this outflow passes through the narrow channel north of Bornholm. From the numerical solution it would appear that slightly more than half of the outflow (or inflow) passes through this channel.

The above results were obtained from a vertically-integrated model with a bottom friction inversely proportional to the square of the depth. Following Platzman 's (1963) formulation for shallow water, the stress coefficient was defined as 2.5 K where K is the vertical eddy viscosity, which was assumed to be of the order of 20 cm^2/s. Although the character of the solutions remains the same for other formulations of bottom friction, some quantitative differences naturally occur. This is illustrated in Figure 6 for selected north-south cross-sections. In all cases the model was run for three days with the wind stress linearly increasing to unity during the first day and thereafter remaining constant. The solid lines were obtained with the same bottom stress formulation as before but assuming a vertical eddy viscosity equal to 40 cm^2/s. The dotted lines represent the solutions for nonlinear bottom friction with a coefficient of $2.5\ 10^{-3}$, which, incidentally, show good agreement with Figures 3 and 4. Finally, the dashed lines of Figure 6 were obtained for the same bottom friction as the solid lines but with the eastern border of the fine mesh model closed. Where the dashed lines are not visible

they coincide with the solid lines, thus indicating that these boundary effects do not propagate very far into the southwest Baltic. However, in the area of the Baltic '75 field program the effects are clearly appreciable, thus requiring an eastward extension of the grid or, as is done here, a nested model of the whole Baltic.

Again, it may be of interest to evaluate the integrated water transport through the channel north of Bornholm as a function of wind direction. This can be done by linear combination of the solutions shown in Figure 3 and 4, and the result is presented in the upper part of Figure 7. It may be recalled that Figures 3 and 4 show the wind-driven circulation in the absence of outflow through the Danish Belts and hence the integrated water transport south of Bornholm would be equal in magnitude but of opposite sign. To put this transport in the proper perspective it may also be recalled that the transport through the same channel, corresponding to the hydraulic flow shown in Figure 5, was about 5.10^4 m^3/s and thus of the same order of magnitude. Furthermore, it should be noted that the integrated transport is a small residual of large opposing currents which is well illustrated by Figure 6.

So far we have essentially eliminated the divergent flow component associated with the free surface oscillations of the whole Baltic, by a judicious application of the model forcing. Under realistic conditions, however, the surface modes are quite apparent and it is important to evaluate the magnitude of the associated currents. From the viewpoint of the fine-

mesh model of the southern Baltic, the surface modes of the Baltic appear as periodic variations of the normal transport through the eastern border of the model. In order to estimate this effect, the nested model was run with a step-function wind stress of unit magnitude and with zero bottom stress. The total transport across the eastern border of the 5-km model, as obtained from the 20 -km model, is shown at the bottom of Figure 7 for a northwind and an east-wind, respectively. The cross-sectional area of this border is of the order of $10^{11} cm^2$ and hence the corresponding velocities are typically of the order of 1 cm/s. The northwind computation was also repeated by simply setting the outflow through the Danish Belts proportional to the local water level with a coefficient based on the earlier observations. This result is shown by the dashed curve in Figure 7.

5. Baroclinic circulations

In this section an attempt is made to estimate the baroclinic effects on the circulation of the southwest Baltic for the type of stratification encountered during the Baltic '75 experiment. Figure 8 shows typical vertical profiles of temperature, salinity, and density in the Bornholm Basin for the spring season. These particular profiles were obtained by averaging observations at 27 stations throughout the Basin, during a ship cruise from May 2 to May 5, 1975. Individual profiles showed only minor deviations from this mean. It is seen that the summer thermocline is starting to develop but its effect on the vertical density distribution is still negligible. Homogeneous conditions prevail from the surface down to depths below 50 m, and it is clear that baroclinic effects should be essentially confined to the area within the 60 m depth contour in Figure 2. It may be recalled that this observation was used previously to justify the purely barotropic boundary conditions at the border between the fine mesh and the coarse mesh.

The density profile of Figure 8 was adopted for the present three-dimensional model computations. Variations of density were predicted from Eq. (1) without any horizontal or vertical diffusion to illustrate advection by currents. In the momentum equations (6) vertical eddy viscosity was confined to the upper homogeneous layers of the 9-layer model. In the 4-layer model the upper layer extended down to 50 m and no eddy viscosity was used. Most computations were carried out with the one-lattice 9-layer model as well as with the one-lattice 4-layer model. For comparison a few calculations were done with the double-lattice grid. As expected, the results from the different models were very similar and there is no need to differentiate between them in our discussion.

Again the models were run for different winds like the barotropic experiments and the results were analyzed after 3 days. For the sake of brevity, however, this discussion will be restricted to a unit wind stress from the northeast, which approximates the true wind episode used for verification in the following section. Furthermore, outflow through the Danish Belts has been included in accordance with observations for the same wind event.

The wind-induced variations of the mass field can be best illustrated by concentrating on the model layer between 60 and 70 m. The density field for this layer after 3 days of NE wind is shown in Figure 9. In order to separate the contributions of the stress-induced vertical velocities from the effects of the topographically-induced vertical-mean flow, the computations were repeated with the latter set equal to zero. This result is shown in Figure 10. The density distribution of Figure 10 will be recognized immediately as the result of surface Ekman drift to the right of the wind and compensating pressure gradient currents below. This is a typical solution for the case where the barotropic and baroclinic flow components can be separated. On the other hand, Figure 9 includes the additional effects of the barotropic flow crossing depth contours with the associated horizontal divergence of the vertical-mean current. Comparison of Figures 9 and 10 shows that such coupling effects of topography and baroclinicity are here at least as large as the separable baroclinic solution. As a result, the response to wind becomes difficult to analyze on the basis of the concepts of conventional baroclinic theory and Ekman dynamics.

In view of the close relationship between vertical variations of the flow field and horizontal gradients of the mass field, the topographic circulation will also affect the internal

This can lead to large variations of water motions within the shallow layer below the maximum density gradient (see Figures 2 and 8). The water transport averaged over the deep homogeneous layer above is very similar to the vertical-mean flow. Thus the baroclinic flow component can be well illustrated by the deviation of the current from the vertical-mean. Such current deviations for the 60-70 m layer are shown in Figures 11 for the case including topographic circulations (compare Figure 9) and in Figure 12 for the case without vertical-mean flow (compare Figure 10). The baroclinic currents are clearly in agreement with the mass field.

Another interesting question is to what extent the vertically-averaged water transport is affected by stratification. It follows from eqs. (7) - (8) that there are two possible effects, namely, a change of bottom stress due to baroclinic currents in the deep layers, and the orientation of the vertically-integrated density anomalies relative to the bottom topography. In the numerical model these effects can be readily separated since the model computes the vertical-mean flow and the vertical shears separately. Thus baroclinicity can be included in the shear equations without allowing for density effects on the mean flow. Such computations were made and the results were compared with multi-layer barotropic solutions. The vertically-averaged flows were essentially indistinguishable, which is not surprising in view of the fact that the bottom stress is less important in deep water. The solution after 3 days of NE wind is shown in Figure 13. This solution is, incidentally, very similar to the solution from a single-layer model with quadratic bottom friction. For comparison, Figure 14 presents the vertical-

mean flow with the density effects included also in the vertically-averaged equations. Substantial changes are found in the stratified part of the basin. Again, the coupling of topography and stratification is apparently not negligible.

In concluding this discussion of hypothetical solutions for the southwest Baltic it may be of interest to consider a few typical current profiles as a function of depth. Such vertical variations can be the result of frictional effects (Ekman currents) or internal pressure gradients (baroclinic currents). Although the corresponding analytical solutions are well known, it is useful to make a quantitative evaluation of these effects for the particular situation which is analyzed in the following section. Let us consider then an elongated channel with a cross-section like the southwest Baltic and a wind along the channel axis such that the stress increases linearly to 1 dyne/cm^2 during the first day and thereafter remains constant. The channel is closed at both ends and hence the surface pressure gradient tends to balance the wind stress integrated over the width of the channel. Consequently, the vertical-mean flow is in the direction of the wind for depths less than the cross-sectional mean and against the wind for larger depths (Bennett, 1973). Figure 15 shows solutions after two days of wind, as obtained from a numerical model with a vertical resolution of 5m. Numbers 0 through 9 indicate levels at 10 m intervals, starting at 5 m depth, such that the solutions 1, 2, 3 may be compared with the Baltic '75 observations at 15, 25 and 35 m, respectively. From left to right, solutions are shown for (a) mean current against the wind, (b) mean current equal to zero, and (c) mean flow in the direction of the wind. The corresponding water depths in the channel model were 95, 65, and 45 m, respectively. From top to bottom, solutions are presented

for (a) homogeneous water with vertical eddy viscosity decreasing linearly from 50 cm^2/s at the surface to zero at 50 m, (b) eddy viscosity twice as large as the above, and (c) original eddy viscosity but including the density stratification of Figure 8. It is clearly demonstrated that, below the upper current meter at 15 m, horizontal variations of computed currents are much larger than vertical variations.

6. Comparison with observations

Verification of model computations requires detailed knowledge of wind forcing as well as current and density observations. It is likely that the most meaningful results will be obtained if one can isolate a particular wind event whose impact on water movements overshadows the effects of regular day-to-day meteorological disturbances. Such a wind episode occurred during the first 10 days of May, 1975. Although the wind speed, measured over water, never exceeded 8m/s, the storm persisted for nearly a whole week with wind direction shifting only slightly from S to SW. Figure 16 shows the relevant part of the wind record taken near current meter mooring 6 (Figure 2) during the Baltic '75 field program. The wind event in the early part of May was adopted for the present verification analysis. In order to minimize effects of erroneous initial conditions, all model runs were started 10 days before the outset of the storm, namely, on April 24, 1975.

The positions of the moored current meters used in this study were shown already in Figure 2. A complete listing of the available current records for this period is presented in Table 1, together with the sounding depths in each station. Station 6 consisted actually of a small-scale array of moorings with horizontal separations of the order of 1 km. For the present purpose, this so-called "inner nest" can be treated as a single station. Individual records within the inner nest and simultaneous drift measurements show reasonably consistent results if proper allowance is made for the different types of instruments used (Schott et al, 1975). The data used here were taken from stations 6A and 6E at the centre of the inner nest. Finally, it should be noted that station 5 was actually numbered mooring 15 during the Baltic '75 field program.

As a first approach to model verification it should be established to what extent the observed water transports can be simulated by a conventional homogeneous storm-surge model. Thus the barotropic nested model discussed in section 4 was run for the period April 24 to May 15, 1975, with outflow through the Danish Belts prescribed on the basis of observations. A quadratic formulation of wind stress was used with a coefficient equal to $1.6\ 10^{-3}$. A linear bottom stress, inversely proportional to the square of the depth with a coefficient of $50cm^2/s$, was incorporated in the first run, approximating Platzman's (1963) solution of the Ekman equations. The results were averaged over 28 hours, eliminating inertial motions with periods of about 14 hours, as well as the major contributions of the free surface modes with periods a little over 1 day (see section 4). Figures 17a-f show synoptic distributions of vertical-mean currents for the first half of May 1975. As before, a vector equal to the grid mesh represents a velocity of 20cm/s. Although the fine mesh model covered the whole southwest Baltic, results are shown only for the Baltic '75 measurement area. Furthermore, every other map has been discarded to reduce the number of figures.

For comparison with these model results, a scheme must be adopted to estimate vertically-integrated water transports from observed currents at 15, 25, 35, 55, and 65 m. In this case it was decided to use the simplest possible averaging procedure consistent with the stratification of Figure 8. Thus a two-layer structure was postulated with an interface depth of 50 m and the flow in the upper (lower) layer equal to the arithmetic mean of all observations above (below) the interface. Again the results were averaged over 28 hours and then entered at the proper locations in Figures 17a-f.

A glance through Figures 17a-f indicates immediately that the observations confirm the basic concept of large-scale vorticity being generated by the interaction of wind stress and bottom slope (see section 2). Thus the clockwise circulation dominating before the storm (Figure17a) is completely reversed by the end of this wind event (Figure 17d). In particular at that time, the agreement between model and observations is remarkably good. Some interesting discrepancies appear in the intermediate Figures, suggesting that the flow reversal in nature occurs slower than in the model. Furthermore, as expected, the correspondence between model results and measurement deteriorates somewhat after the storm, when the flow breaks up in a number of counter-rotating cells moving around the basin (Figures 17e-f). Such circulation cells are typically found in the so-called topographic modes of oscillation of a basin with irregular bottom topography.

For a more detailed analysis and verification it is convenient to consider time series of observed and computed currents as a function of depth for given locations. Here results will be presented from the 9-layer baroclinic model with uniform layer depths of 10 m. The model was started from rest on April 24, 1975, with the density distribution shown in Figure 8. Computed currents were simply taken from model grid points closest to the corresponding observation stations. Again the currents are averaged over 28 hours for this comparison.

The upper part of Figure 18 shows results for station 1 along the northern shore of the Bornholm Channel. Here the water depth is only 48 m and the vertical variation of currents with depth is essentially due to frictional effects only. Apparently, this vertical shear is very well simulated by the model, thus indicating that eddy viscosity effects are properly taken into account. However, during the first half

of the storm, the observations suggest a vertical-mean flow in northerly direction (against the wind), whereas the model computes a southward transport. Recalling that the model computes vertical-mean flow and vertical shears separately, it appears clear that possible improvement of this result can be achieved only by a better simulation of the barotropic flow component, i.e., the balance between surface pressure gradient and wind and bottom stresses.

The lower part of Figure 18 presents results for station 2 in the middle of the Bornholm Channel. To facilitate a visual comparison of observations and model results, currents are shown only for 15, 35, and 65m. A two-layer structure is clearly indicated, with only minor vertical shears within the upper layer. The vertical shears between 35 and 65 m are almost completely due to baroclinic effects. This was verified by running the same model without stratification. Thus these observations tend to support the baroclinic computations discussed in the previous section. In this case, the vertically integrated transport also appears quite well reproduced by the model, thus confirming that the transport in deep water tends to run against the wind.

More complicated appears the observed water circulation along the shore of Bornholm Island, in particular in station 4. This is shown in the upper part of Figure 19. Again, at the beginning of the storm, May 4-5, there is a tendency for the model to properly reproduce the baroclinic shears between upper and lower layers, although the observed shearing motions are substantially larger in magnitude. Most surprising, however, is the sudden increase of current velocities throughout the upper homogeneous layer. Since the local water depth is only 64m, it appears likely that there is a large net water

transport in northerly direction along the shore. This could tie in with the northerly flow at station 1 for the same period, May 5-8. It may be noted that this longshore transport is at right angles to the wind and,consequently, the direct effect of the wind stress on this component of the vertically-integrated flow should be negligible. This would point at the surface pressure as the source of the observed accelerations. At any rate, the phenomenon disappears as suddenly as it appeared and the subsequent currents are remarkably similar in the model and in nature.

The remaining shallow water stations, 5, 10, and 11, behave typically like station 1 (see also figure 17). In all these stations the agreement between model and observations appears acceptable. The deep water stations (6, 7, 9) show a quite different pattern. As an example, station 6 is shown in the lower part of Figure 19. In this case, as for all offshore stations, the prevailing direction of the water transport is against the wind, but the magnitude of the observed currents is consistently underestimated by the model. The difference can be largely traced to erroneous initial conditions. Even though the model was started 10 days before the storm, the computed deep water circulation at the onset of the storm appears much weaker than the observed water movements. It should be noted, however, that there are indications that the moored current meters overestimated actual current speeds. Thus, drift measurements by Schott et al (1975) for this storm period and this area show mean speeds of about 5cm/s and directions varying from N to NE between the surface and 30m. The observed currents in station 6 are about twice as large, the computed ones about half as large as the drifters indicate.

All in all it is evident that it would be a difficult task to properly model the circulation of the deep basin. As demonstrated by the numerical results of Figure 17, the circulation consists of closed cells which migrate continually through the basin. The currents at any given point depend on its position relative to these cells and small errors in position will lead to completely different currents in a model gridpoint which is used for verification. Thereby comes that water movements in this deep, stratified basin can persist for very long times so that observed circulations cannot be related to known forcing functions in a straightforward manner. This leads to a build-up of momentum and is probably the reason for the discrepancies between model and observations with regard to current speeds in deep water.

This discussion will be concluded with a few remarks on density variations. In view of the magnitude of the density gradient at the salinity interface (Figure 8), appreciable pressure gradients will be associated with even the smallest changes in the position of the interface. It is, therefore, practically impossible to properly describe the dynamic configuration of the interface on the basis of observations. Hence, the model runs were started from a horizontally-uniform density distribution. Now the time-variation of density at a given station can be compared with a corresponding point in the model. The problem is then that observed changes may be affected by advection of horizontal variations of temperature and salinity, which are excluded from the model results by the initial conditions. Near the shores, however, one would expect that such effects are most likely overshadowed by vertical advections. Thus Figure 20 shows observed and computed density variations, at the level closest to the maximum density gradient, for stations 3 and 4 along the shore of Bornholm Island. The time variations suggest that vertical displacements in this area are reasonably well simulated.

Acknowledgements

This research was supported by the Fraunhofer-Gesellschaft, München, and by the Program of Canadian-German Collaboration in Oceanography. Computer time was made available by the University Computing Centre, Kiel.

The author gratefully acknowledges the valuable help and advice from the staff of the Institut für Meereskunde, in particular, Prof. W. Krauss, Mr. J. Kielmann, Mr. J. Holtorff, and Ms. D. Raasch.

References

BENNETT, J.R. 1973: On the dynamics of wind-driven lake currents. J. Phys. Oceanogr., 4, 400-414.

BRYAN, K., 1969: A numerical method for the study of ocean circulation. J. Computat. Phys., 4, 347-376.

CHARNEY, J.G., 1955: Generation of oceanic currents by wind. J. Marine Res., 14, 477-498.

CHEN, J.H., and K. MIYAKODA, 1974: A nested grid computation for the barotropic free surface atmosphere. Mon. Wea. Rev., 102, 181-190.

CSANADY, G.T., 1973: Transverse internal seiches in large oblong lakes and marginal seas. J. Phys. Oceanogr., 3, 439-447.

ELVIUS, T., and A. SUNDSTROM, 1973: Computationally efficient schemes and boundary conditions for a fine-mesh barotropic model based on the shallow water equations. Tellus, 25, 132-156.

GROEN, P., and G.W. GROVES, 1962: Surges. The Sea, vol.1, M.N. Hill, Ed., New York, Interscience, 611-647.

HANSEN, W., 1956: Theorie zur Errechnung des Wasserstandes und der Strömungen in Randmeeren nebst Anwendungen. Tellus, 8, 287-300.

HOLLAND, W.R., 1973: Baroclinic and topographic influences on the transport in western boundary currents. Geophys. Fluid Dyn., 4, 187-210.

JACOBSEN, T., 1976: Preliminary transport calculations in the Great Belt. Proc. 10th Conf. Baltic Oceanogr., Göteborg, June 2-4, 1976.

KEUNECKE, K.H., H. Kohn, W. Krauss, G. Miosga, F. Schott, P. Speth, J. Willebrand, W. Zenk, 1975: BALTIC 75, Physikalischer Teil. Institut für Meereskunde, Universität Kiel, Bericht Nr. 11, 100 pp.

KIELMANN, J., 1976: Numerical modelling in connection with Baltic 75. Proc. 10th Conf. Baltic Oceanogr., Göteborg, June 2-4, 1976.

KRAUSS, W., and L. MAGAARD, 1962: Zum System der Eigenschwingungen der Ostsee. Kieler Meeresforschungen, 18, 184-186.

NATIONAL ACADEMY OF SCIENCES, 1975: Numerical Models of Ocean Circulation. Proc. Symp. Durham, N.H., October 17-20, 1972, 362 pp.

PHILLIPS, N.A., and J. SHUKLA, 1973: On the strategy of combining coarse and fine grid meshes in numerical weather prediction. J. Appl. Meteor., 12, 763-770.

PLATZMAN, G.W., 1963: The dynamical prediction of wind tides on Lake Erie. Meteor. Monogr., 4, No. 26, 44pp.

RAO, D.B., and T.S. MURTY, 1970: Calculations of the steady state wind-driven circulation in Lake Ontario. Arch. Meteor. Geophys. Bioklim., A19, 195-210.

REID, R.O., 1975: Analytical and numerical studies of ocean circulation. Rev. Geophys. Space Phys., 13, 607-609.

SCHOTT, F., M. Ehlers, L.M. Hubrich, D. Quadfasel, 1976: On measurements of horizontal mass and momentum transfer in small scales during BALTIC 75. Institut für Meereskunde, Universität Kiel, 45 pp.

SIMONS, T.J., 1974: Verification of numerical models of Lake Ontario. Part 1: Circulation in spring and early summer. J. Phys. Oceanogr., 4, 507-523.

WELANDER, P., 1959: On the vertically integrated mass transport in the oceans. The Atmosphere and the Sea in Motior B. Bolin, Ed., 95-101.

Figure Captions

Figure 1. Baltic Sea with area of fine-mesh models indicated by shading. Dark shading indicates baroclinic model, light shading represents barotropic fine-mesh model.

Figure 2. Topography of SW Baltic (corresponding to dark shading in Figure 1) and positions of moored instruments during BALTIC 75 field program.

Figure 3. Wind-driven circulation after 3 days of unit wind stress from the north. Vector equal to one grid spacing represents a vertical-mean velocity of 20 cm/s.

Figure 4. Same as Figure 3 but for wind from the east.

Figure 5. Hydraulic circulation after 3 days of outflow through the Danish Belts equal to $10^5 m^3/s$.

Figure 6. Wind-driven barotropic flow for selected cross-sections after three days of unit wind stress. Solid lines for linear bottom friction, dotted lines for nonlinear bottom drag, dashed lines for closed eastern border of fine mesh.

Figure 7. Above: integrated water transport through Bornholm Channel for unit wind stress and without outflow through the Danish Belts.
Below: integrated water transport through eastern border of southwest Baltic for step function wind of unit magnitude, in the absence of outflow through Danish Belts and without bottom friction. Dashed curve represents solution with outflow proportional to water level at western shore.

Figure 8. Vertical profiles of temperature, salinity, and density for Bornholm Basin in early May, 1975.

Figure 9. Density anonomaly for model layer between 60 and 70 m after three days of NE wind with realistic outflow through Danish Belts.

Figure 10. Same as Figure 9 but excluding effects of vertical mean topographic circulation.

Figure 11. Deviations of currents from vertical-means for the same depths and flow conditions as Figure 9.

Figure 12. Same as Figure 11 but corresponding to conditions of Figure 10.

Figure 13. Vertical-mean currents after 3 days of NE-wind obtained from baroclinic model excluding density effects on vertically-integrated flow component.

Figure 14. Same as Figure 13 but including all density effects.

Figure 15. Typical current profiles as a function of depth at uniform intervals between 5 and 95m, indicated by numbers 0 through 9. From left to right: mean currents against the wind, equal to zero, and in the direction of the wind, respectively. From top to bottom: barotropic with eddy viscosity of 50 cm^2/s at the surface, same with eddy viscosity doubled, and baroclinic with stratification of Figure 8.

Figure 16. Wind measured over water at position of mooring 6 during BALTIC 75 (Figure 2).

Figure 17. Synoptic distributions of vertical mean currents computed with a barotropic model (light arrows), together with corresponding currents estimated from observations (double arrows).

Figure 18. Observed and computed currents, averaged over 28 hours, for station 1 (above) and station 2 (below) in the Bornholm Channel.

Figure 19. Same as Figure 18 but for nearshore station 4 (above) and offshore station 6 (below)

Figure 20. Observed and computed density variations at lowest observation level for stations 3 and 4 along the shore of Bornholm Island.

Table 1: Moored current meters during period May 1-15, 1975.

Position	Water depth	Instrument depths (in meters)				
1	48	15		35		
2	78	15	25	35	55	65
3	69	16	26	36		65
4	64	15	25	35	55	61
5	55	15		35		
6	74	approx. 25 current meters in 7 moorings				
7	69		25	35	55	64
9	70	15		35	55	65
10	61		25	35	55	
11	38		25	35		

Fig.1

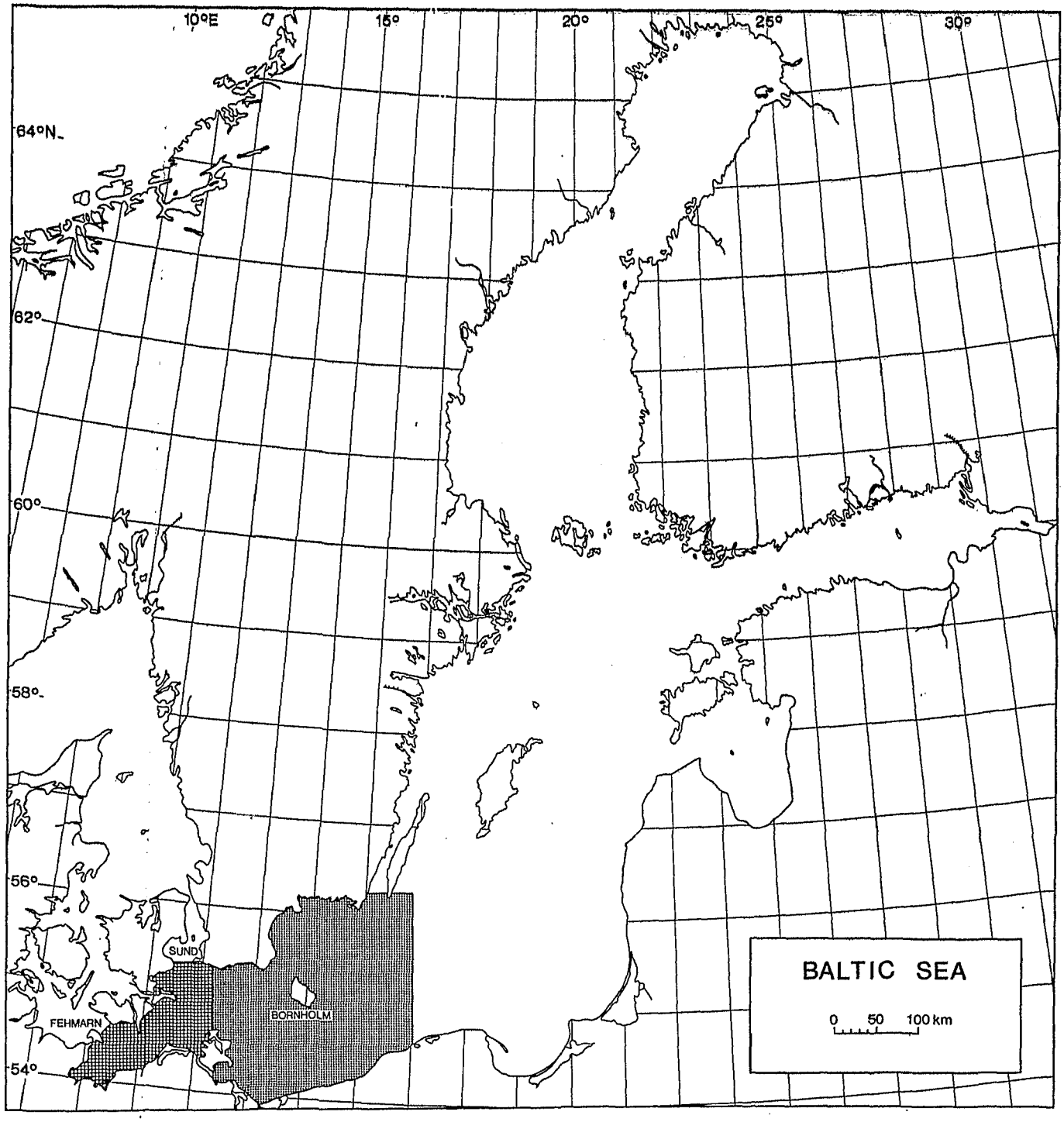
10°E
15°
20°
25°
30°
64°N
62°
60°
58°
56°
54°
SUND
FEHMARN
BORNHOLM
BALTIC SEA
0 50 100 km

Fig.2

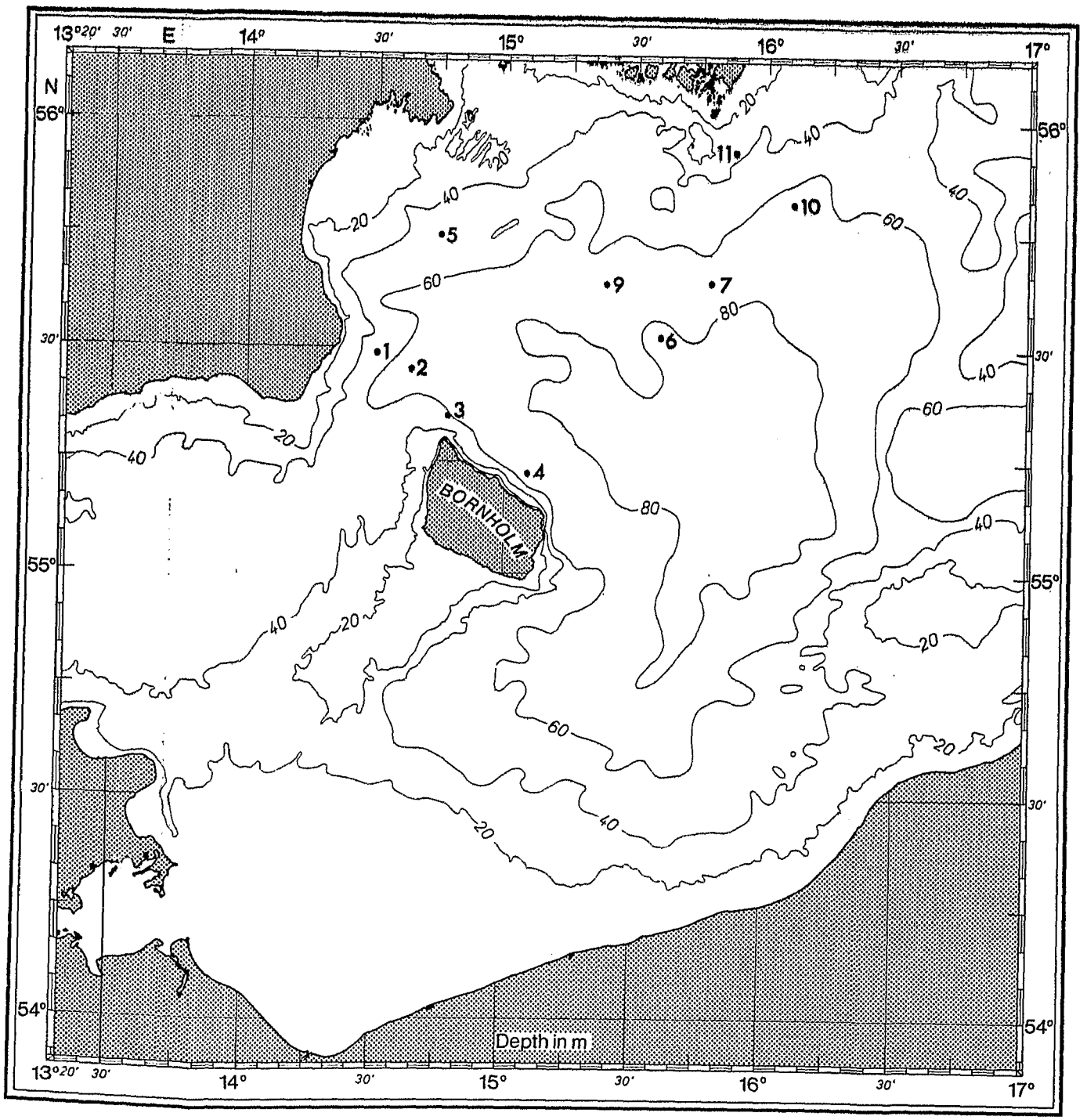
13°20' 30' E
14°
30'
15°
30'
16°
30'
17°
N
56°
30'
55°
30'
54°
BORNHOLM
1
2
3
4
5
6
7
9
10
11
20
40
60
80
Depth in m

Fig.3

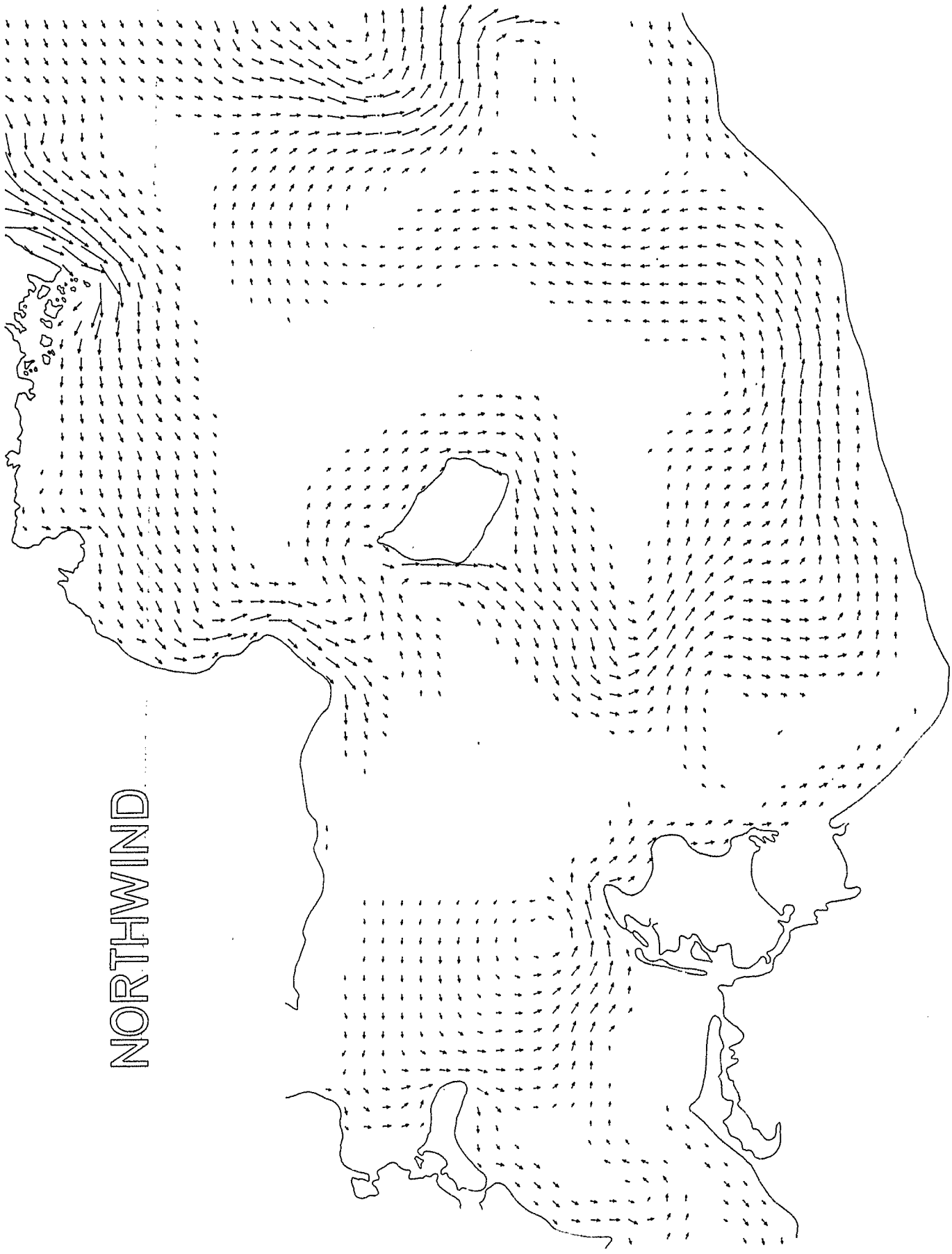

Fig.4

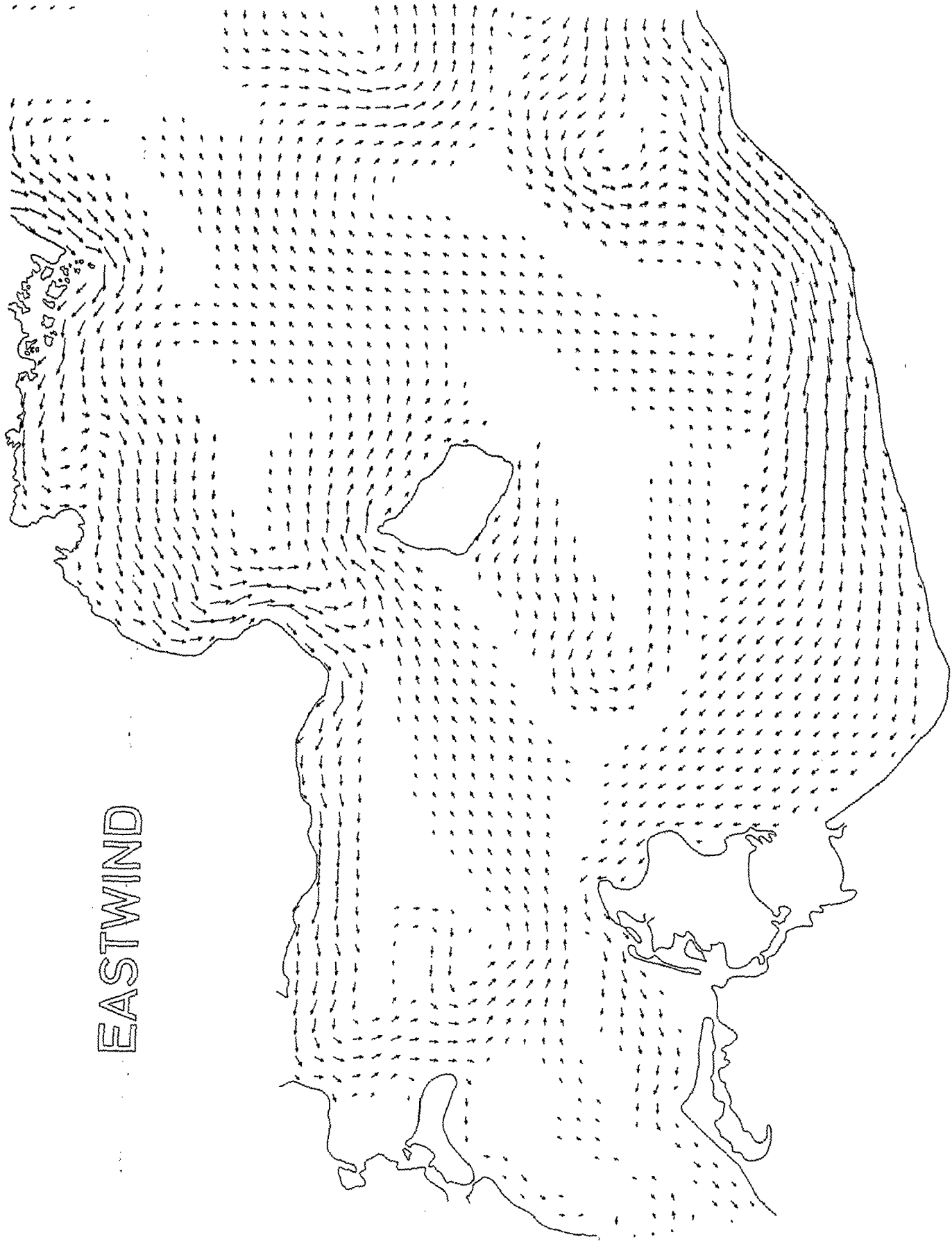

Fig.5

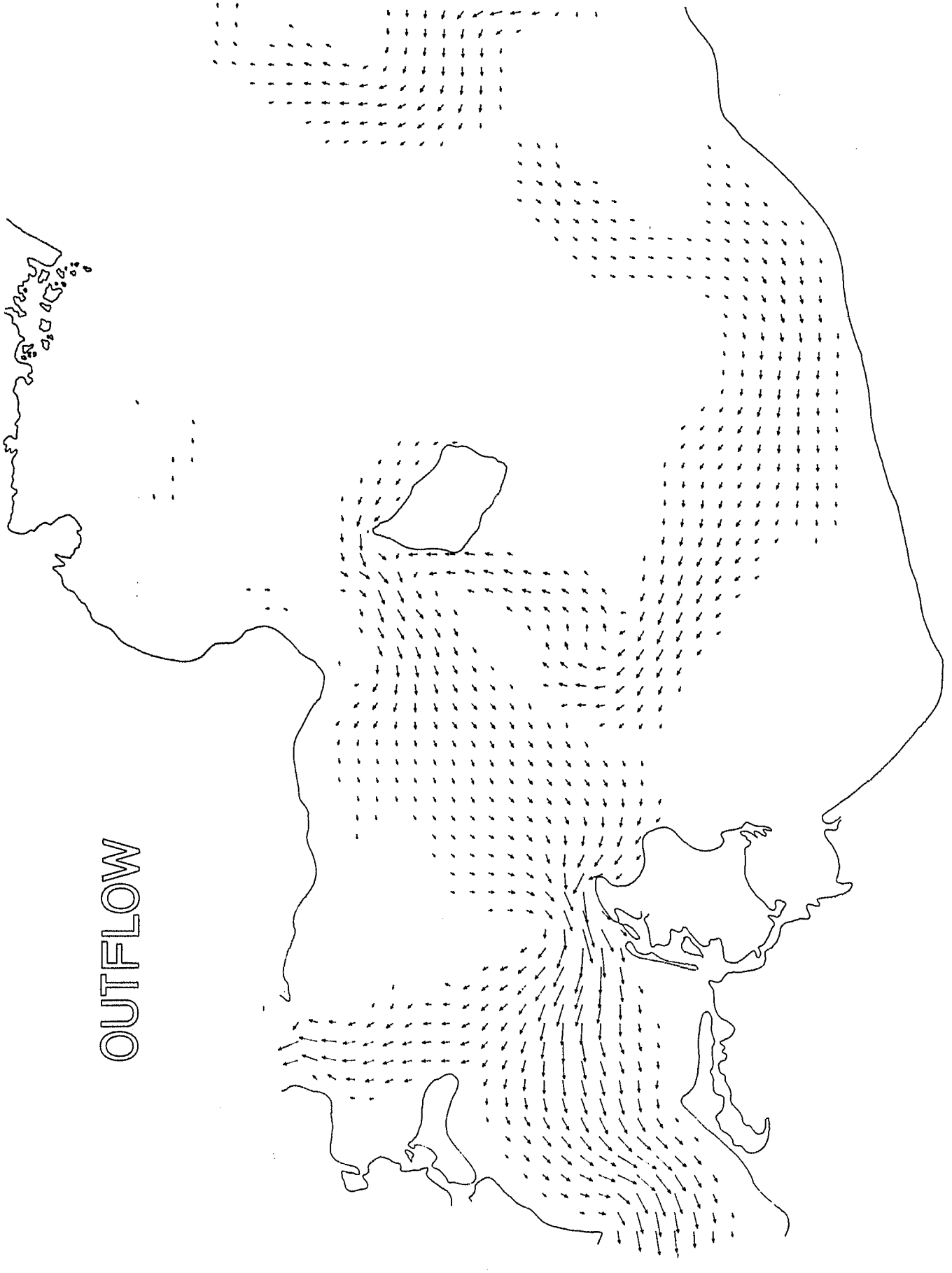

Fig.6

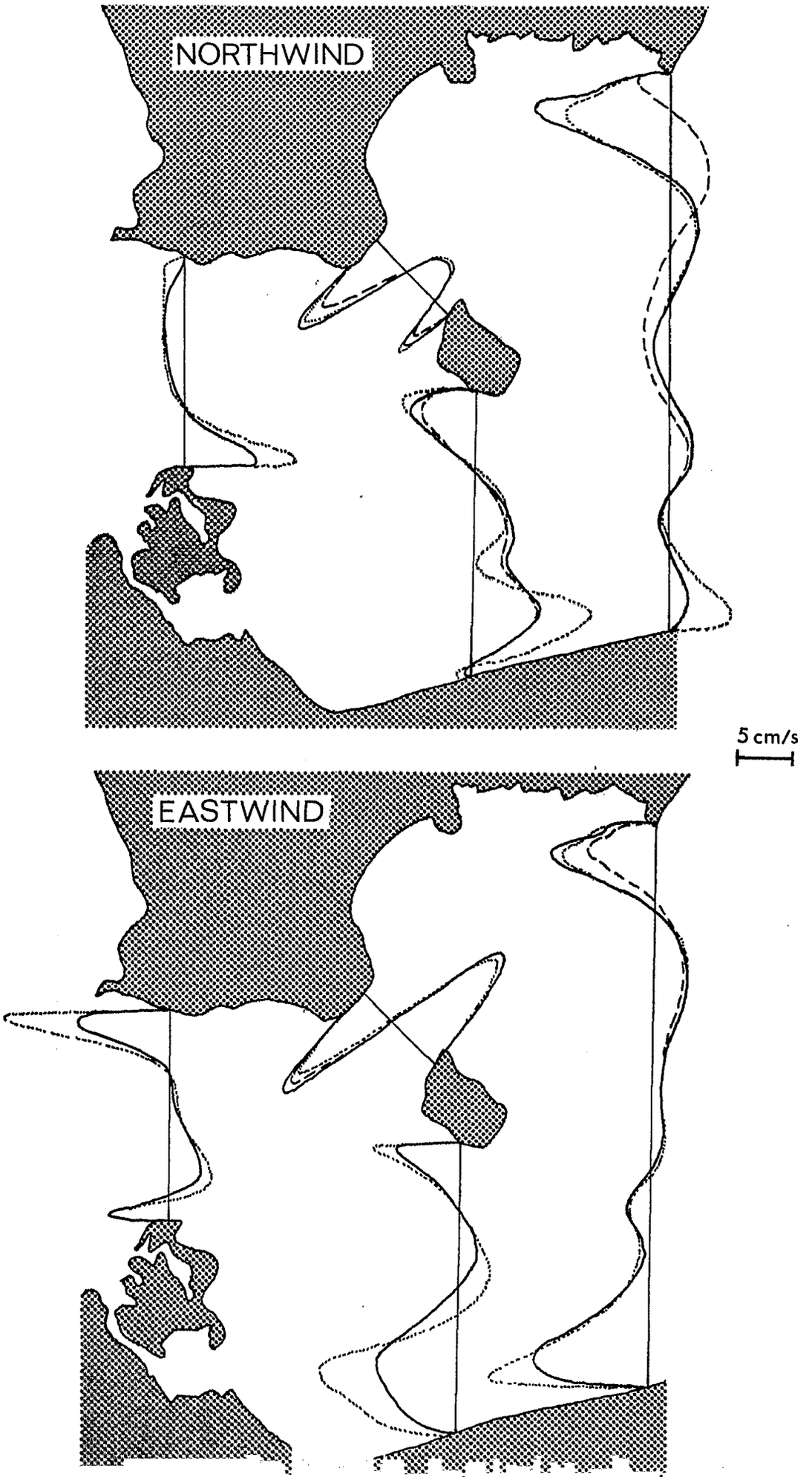

Fig.7

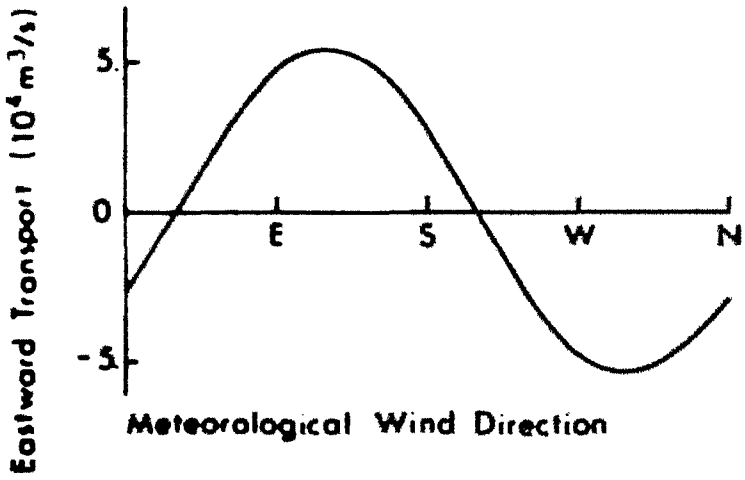
Eastward Transport ($10^4 m^3/s$)
5
0
-5
E
S
W
N
Meteorological Wind Direction

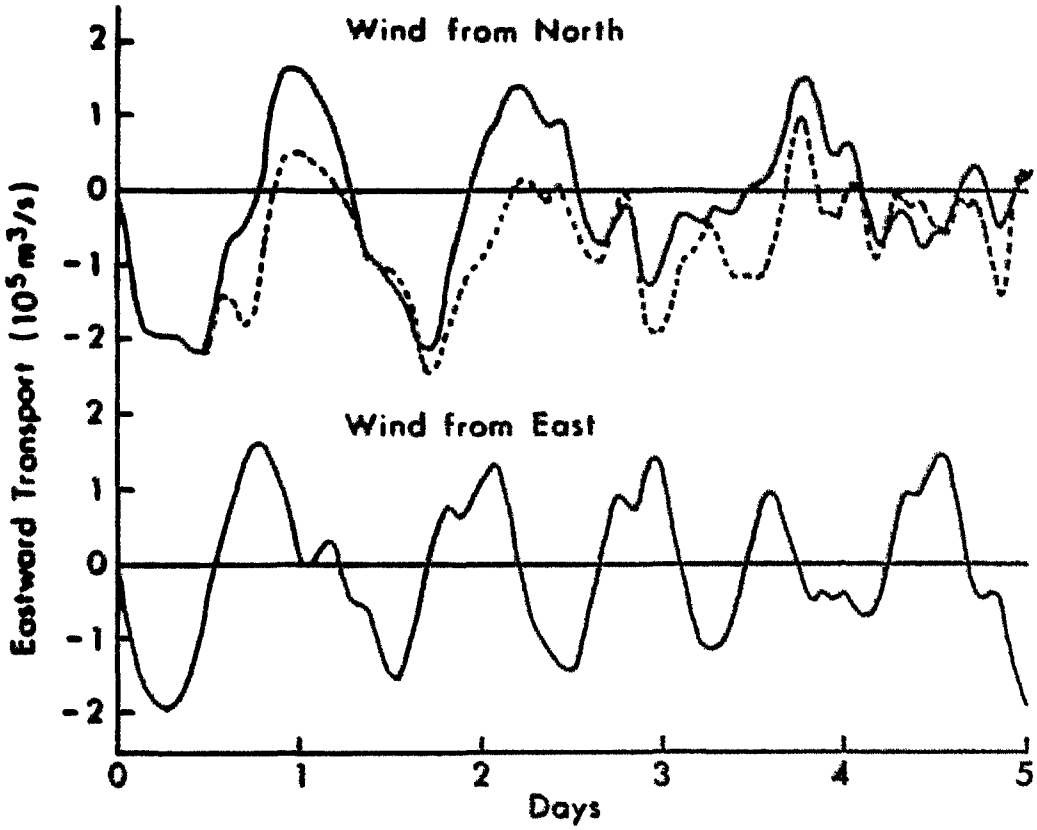
Wind from North
Wind from East
Eastward Transport ($10^5 m^3/s$)
2
1
0
-1
-2
0
1
2
3
4
5
Days

Fig. 8

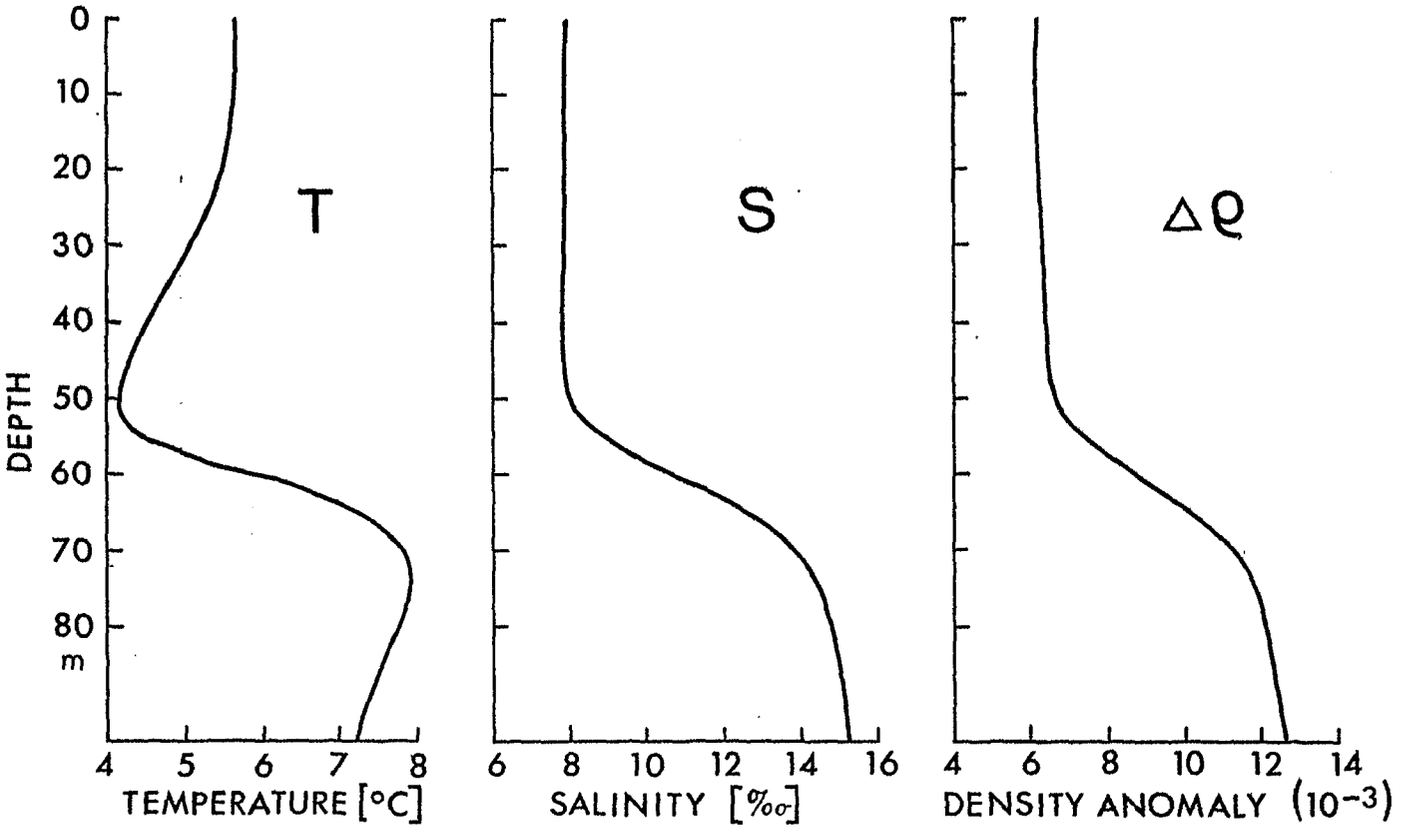
DEPTH
0
10
20
30
40
50
60
70
80
m
T
S
ΔQ
4 5 6 7 8
TEMPERATURE [°C]
6 8 10 12 14 16
SALINITY [‰]
4 6 8 10 12 14
DENSITY ANOMALY (10⁻³)

Fig. 9

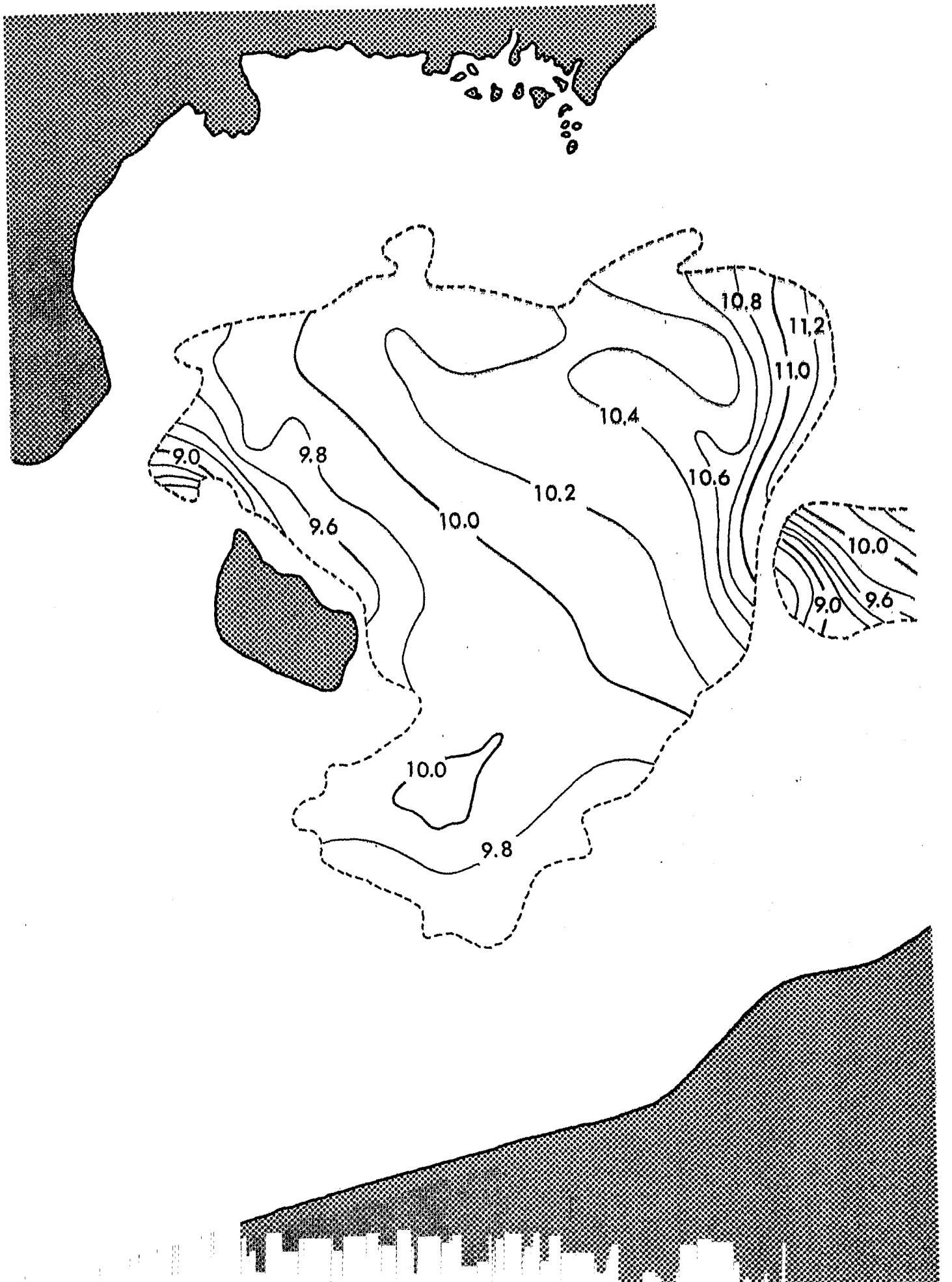

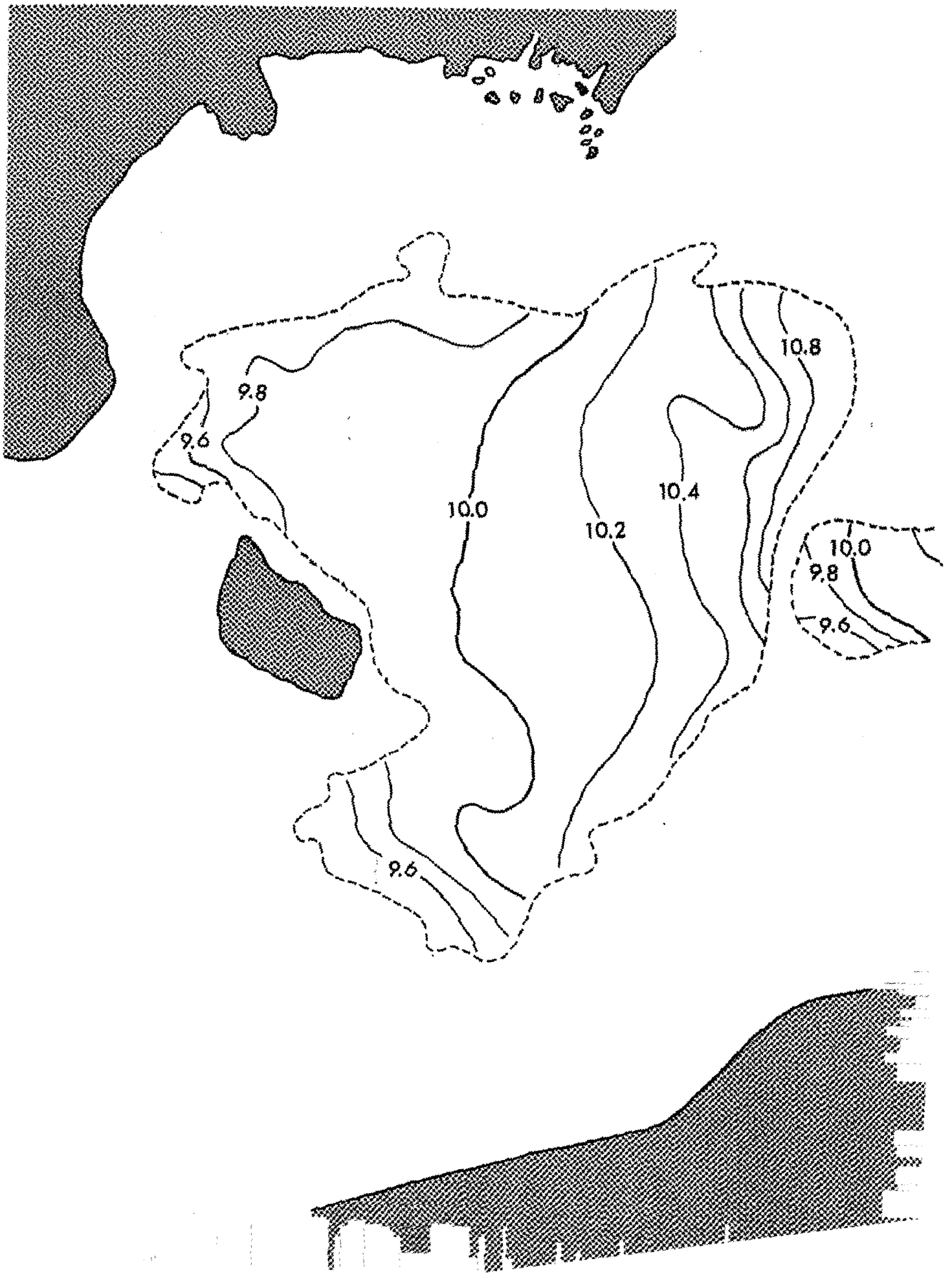
9.6
9.8
10.0
10.2
10.4
10.8
9.6
9.8
10.0

Fig.11

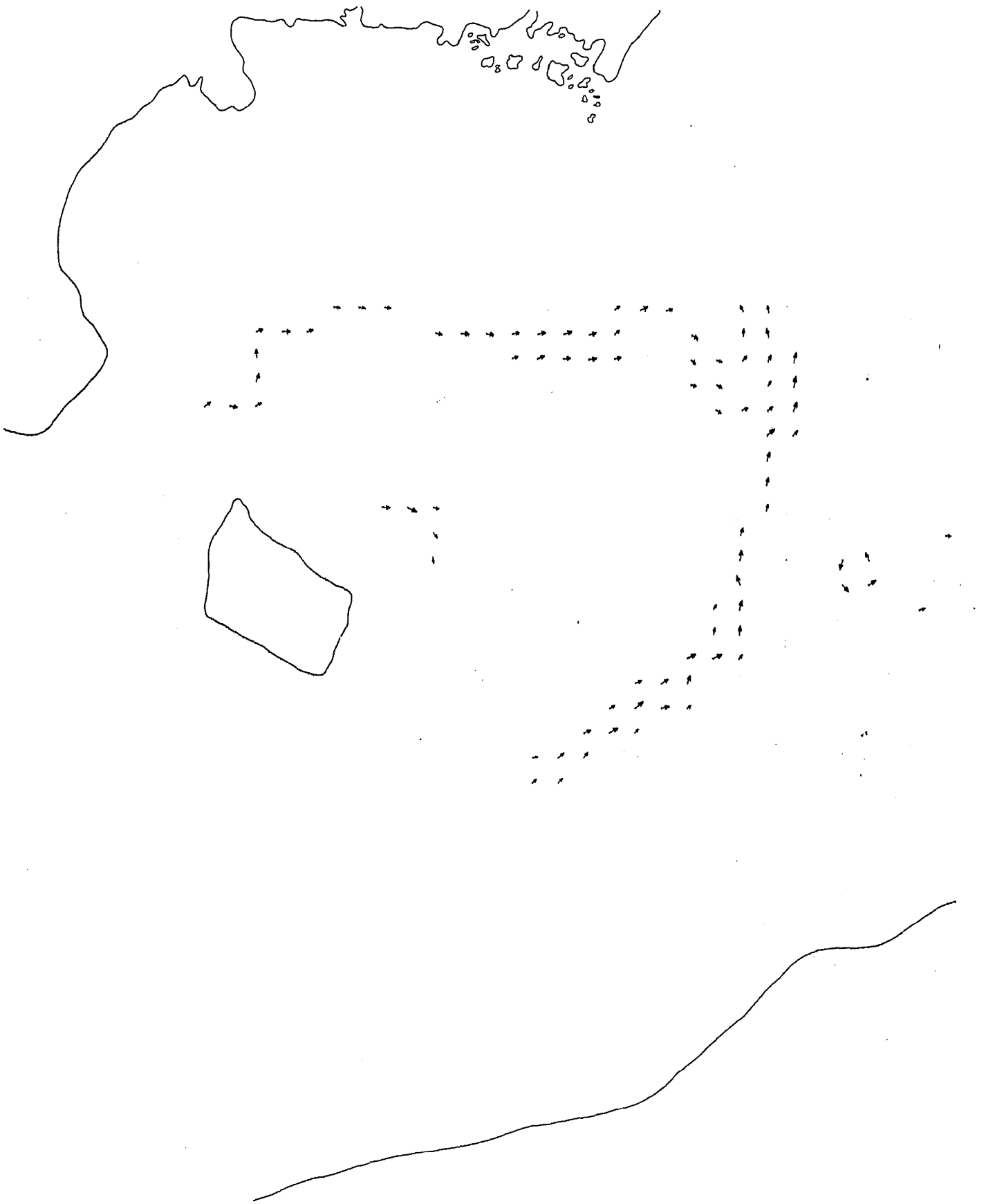

Fig.12

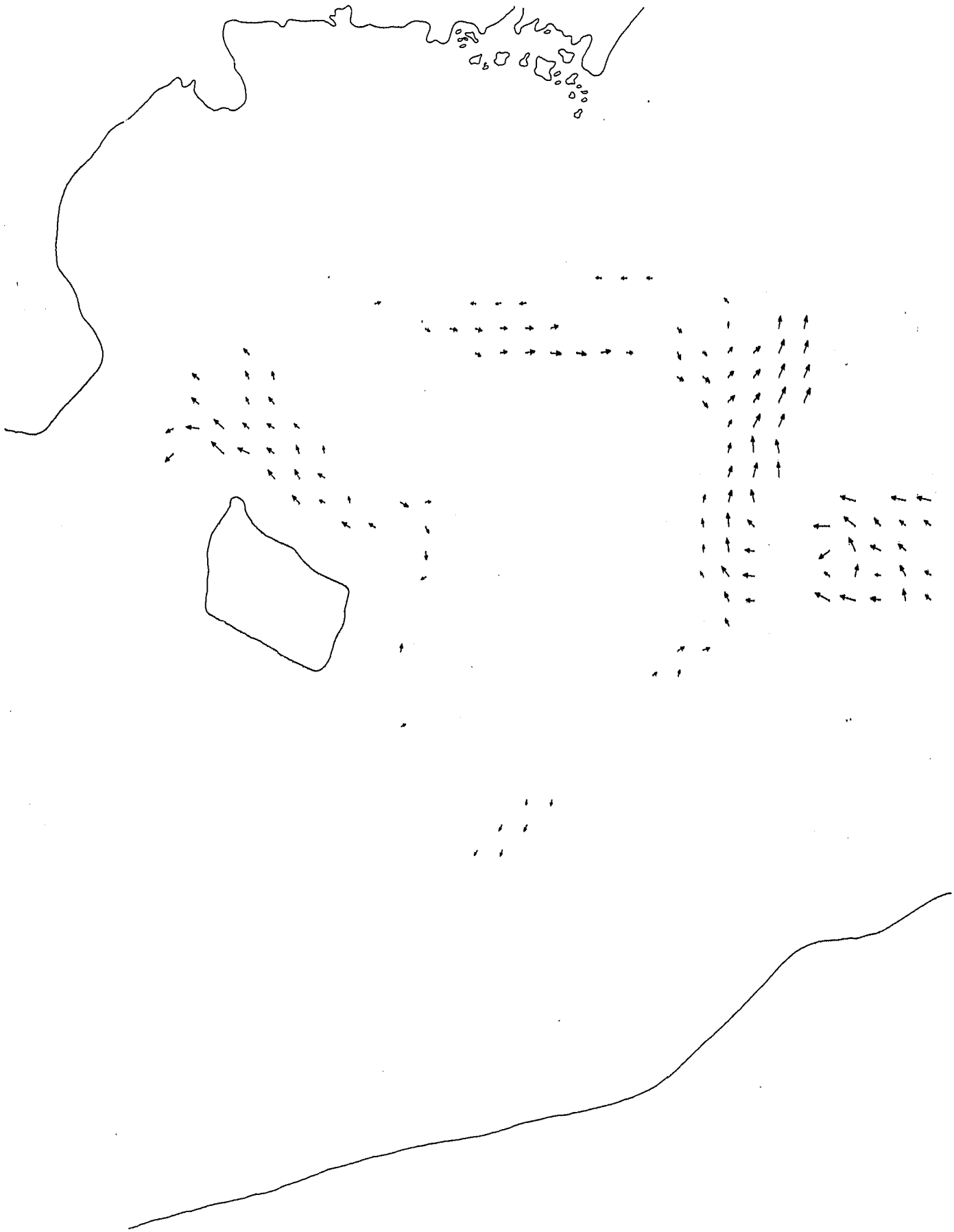

Fig.13

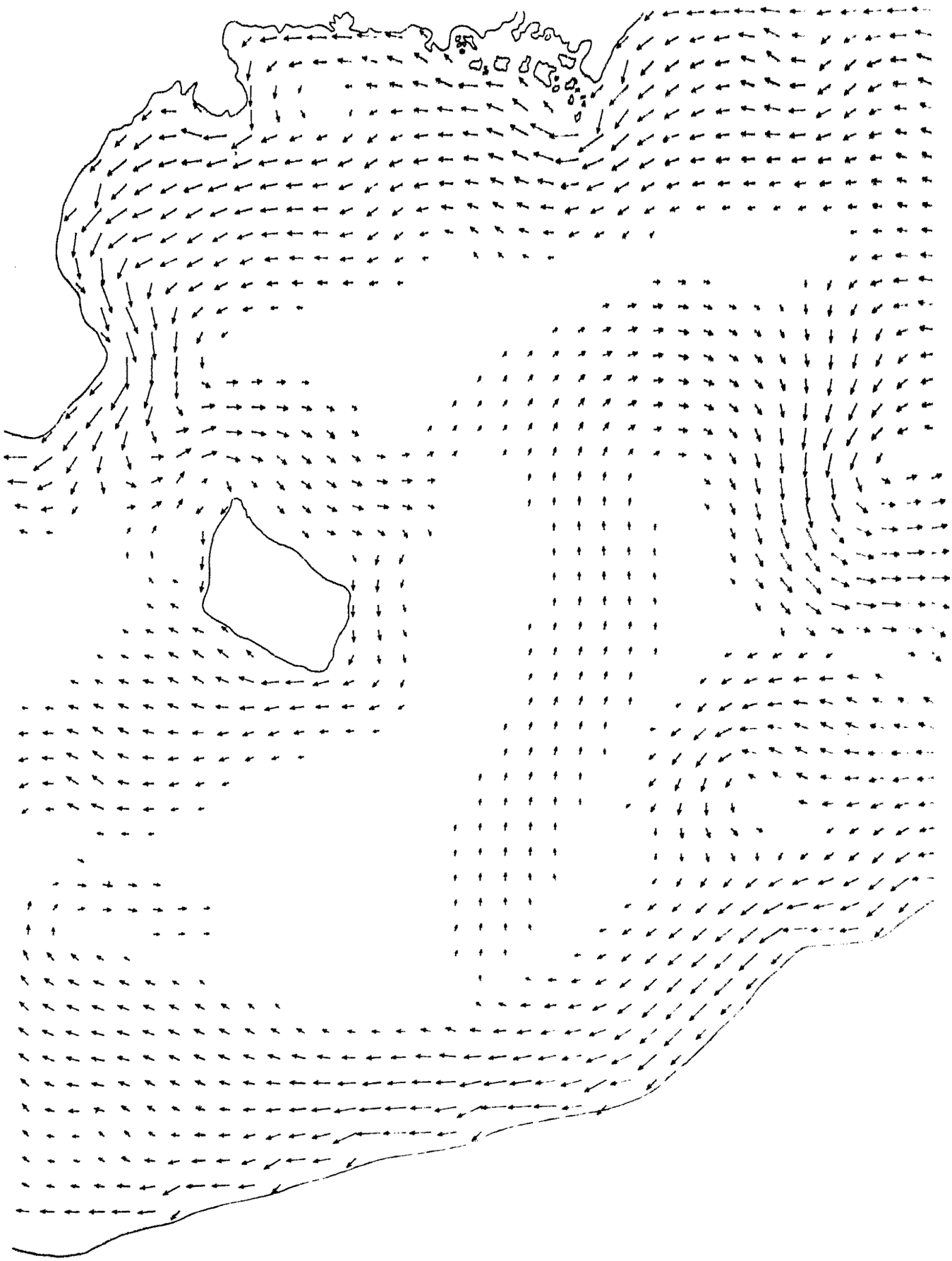

Fig. 14

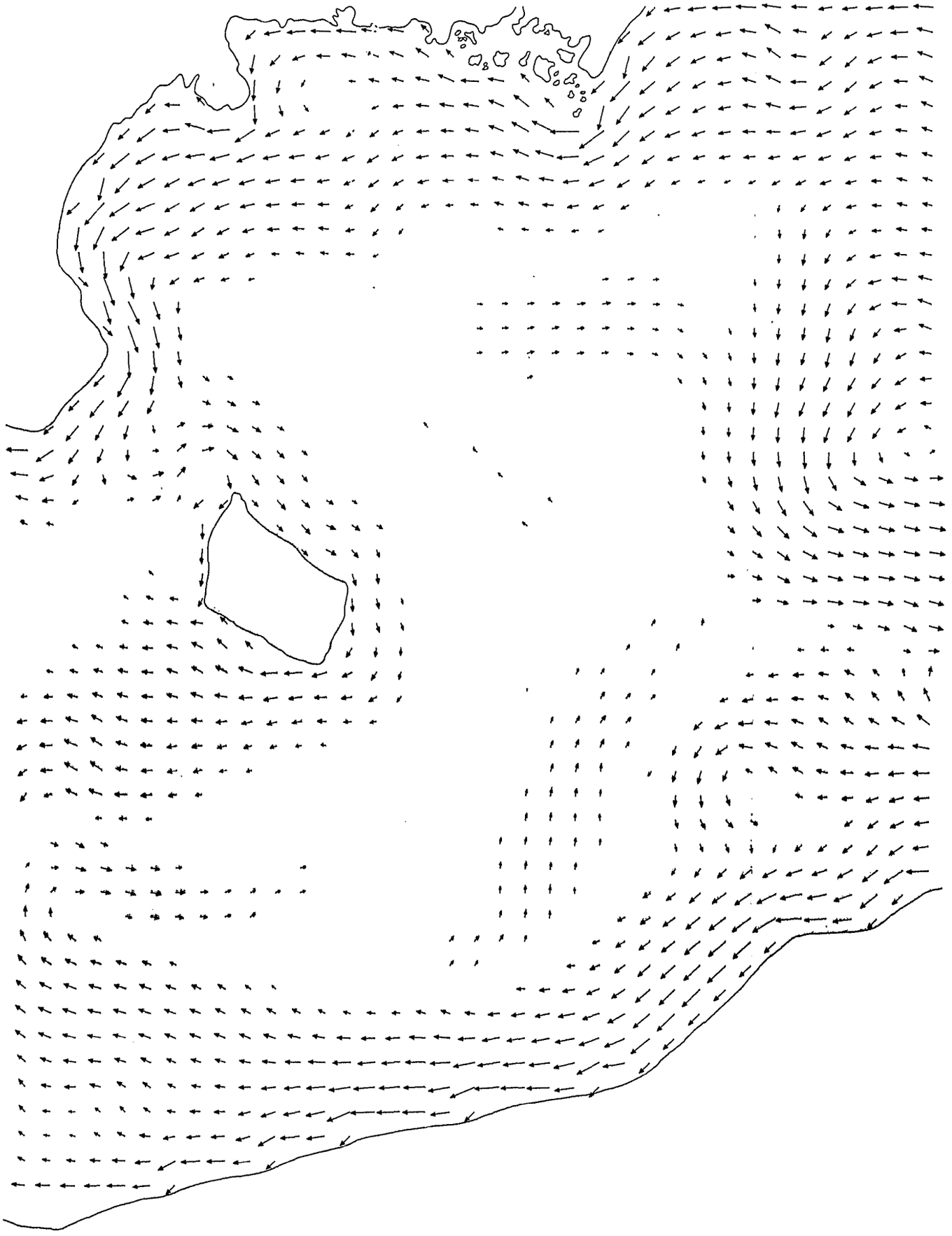

Fig. 15

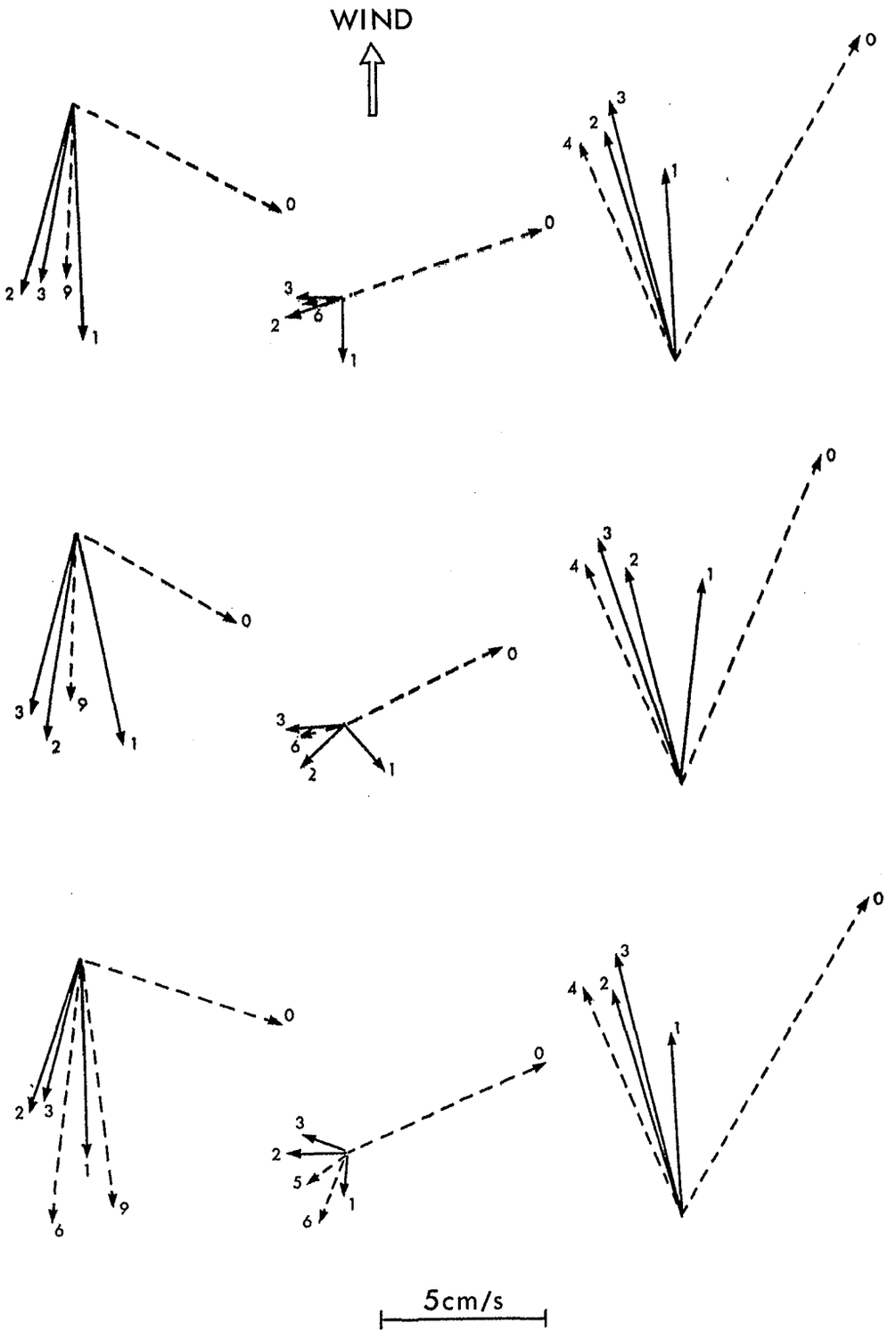

Fig.16

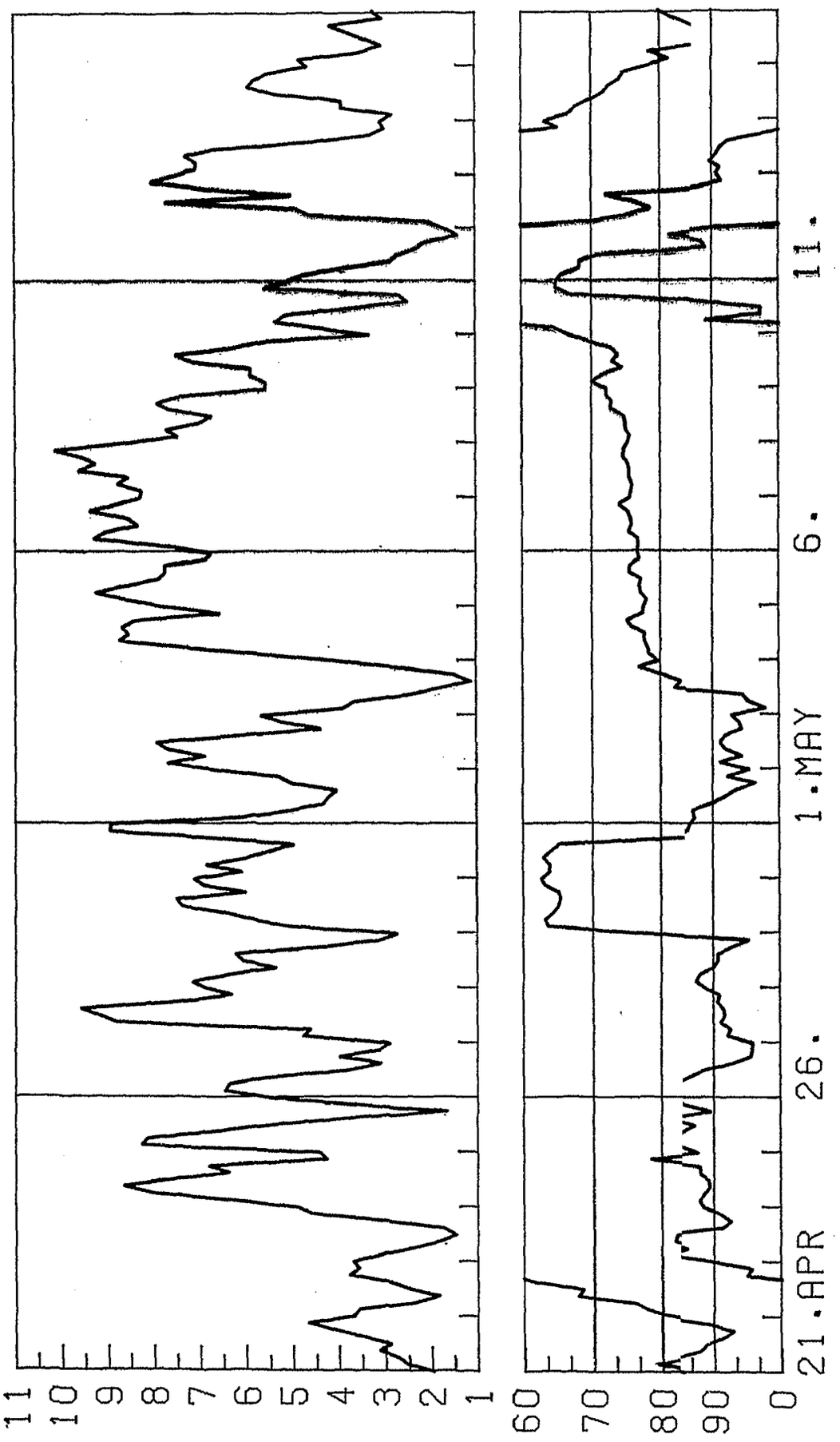

Fig.17a

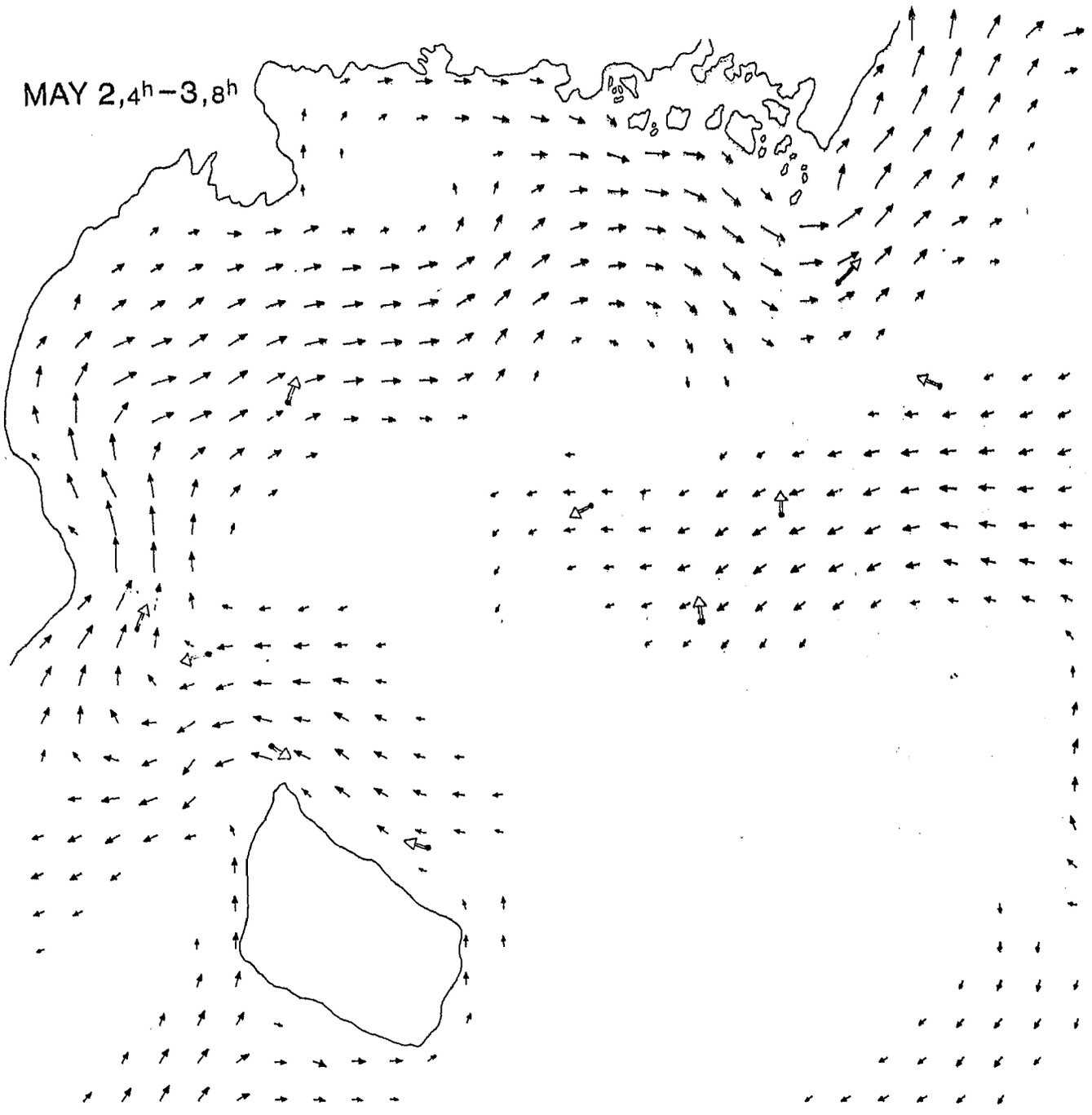

Fig. 17b

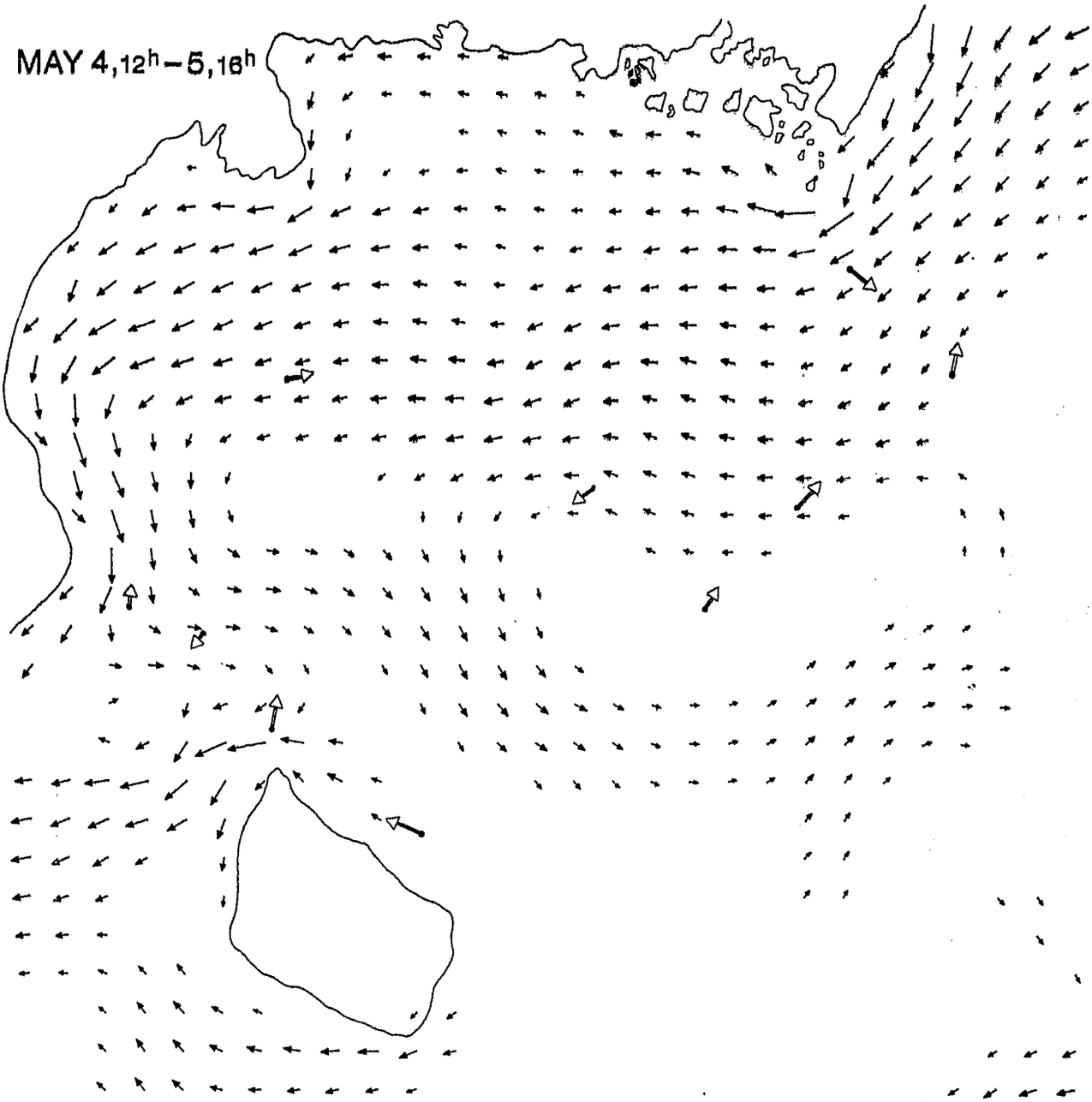

Fig. 17c

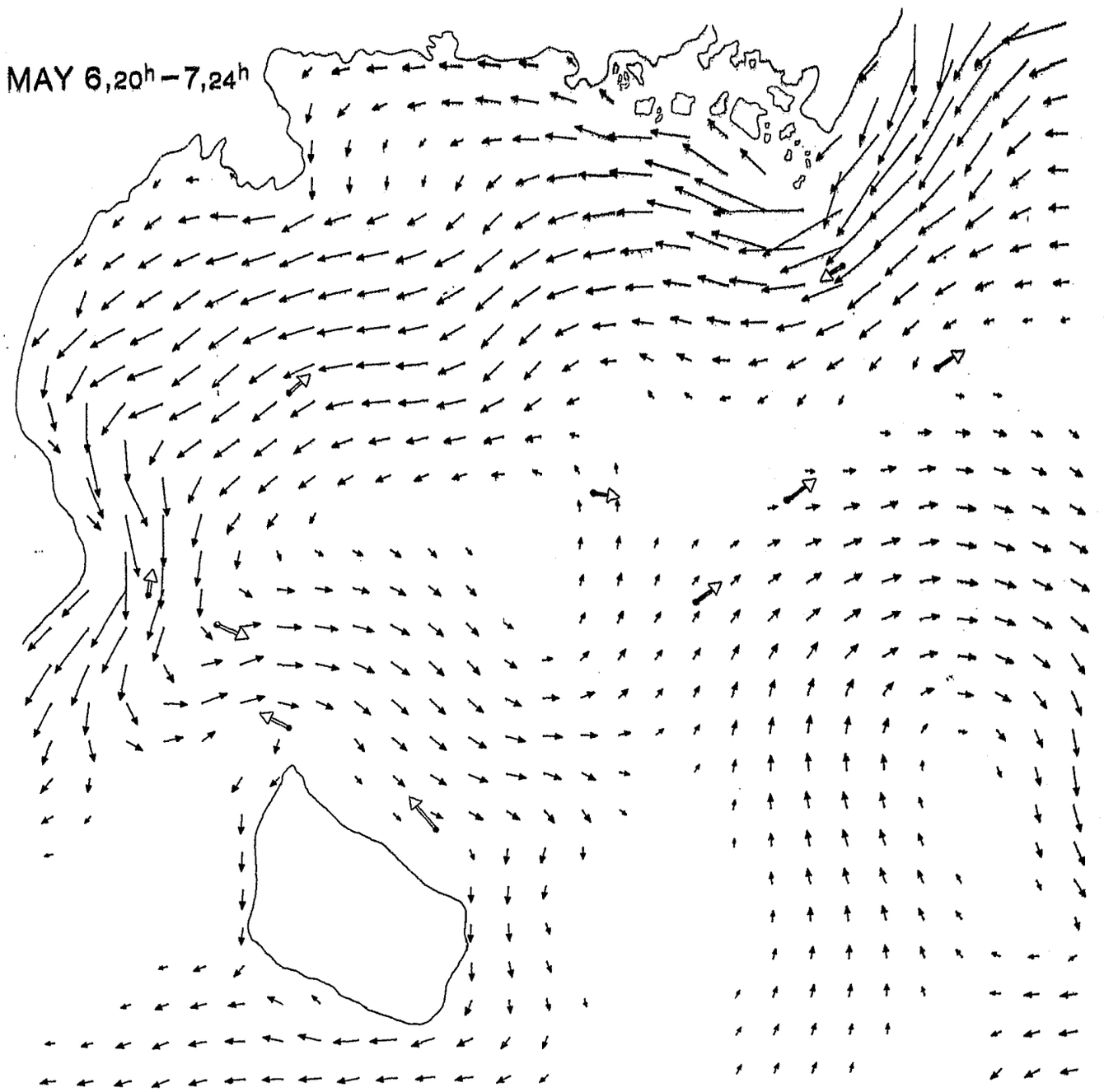

Fig.17d

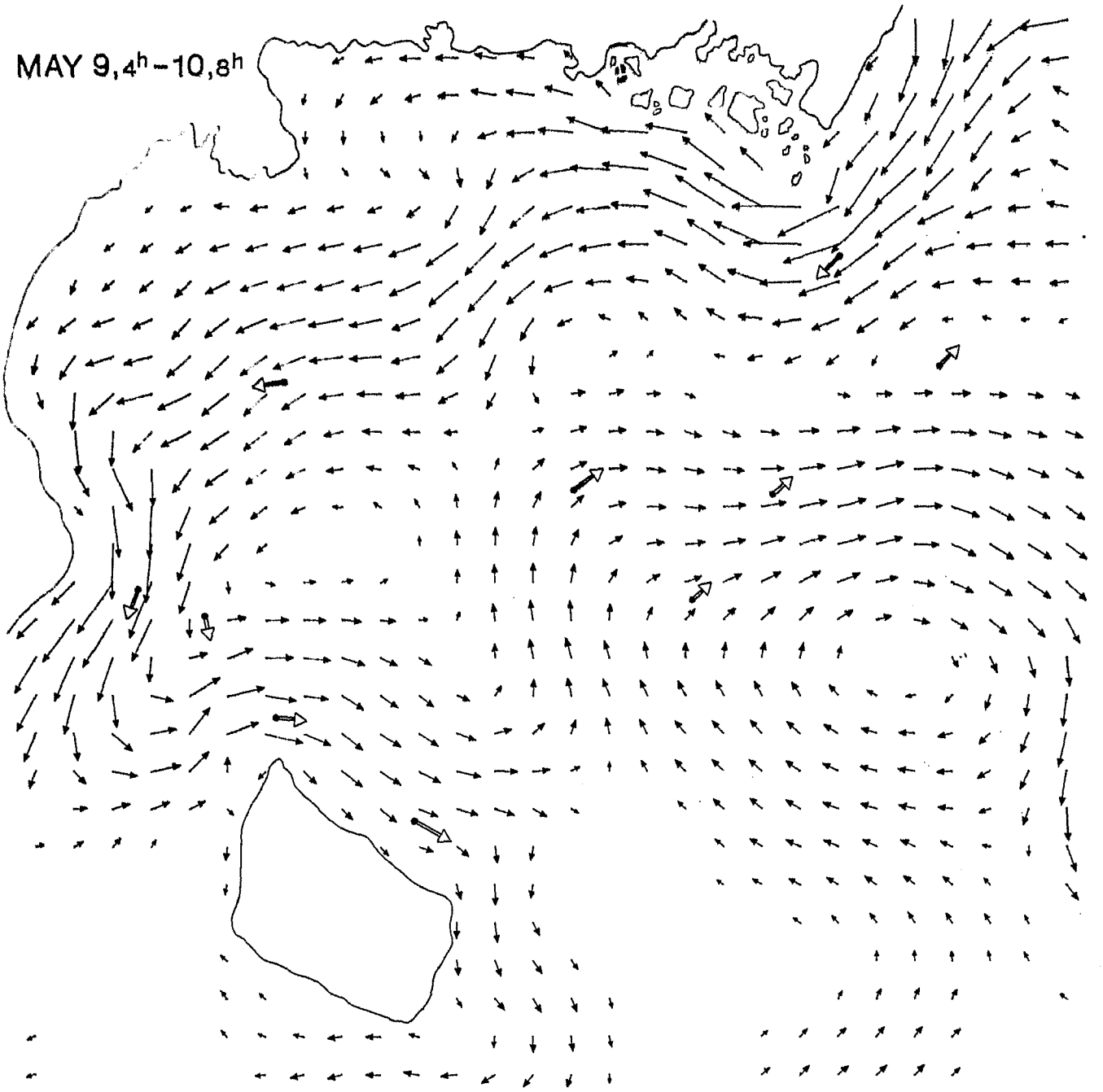

Fig.17e

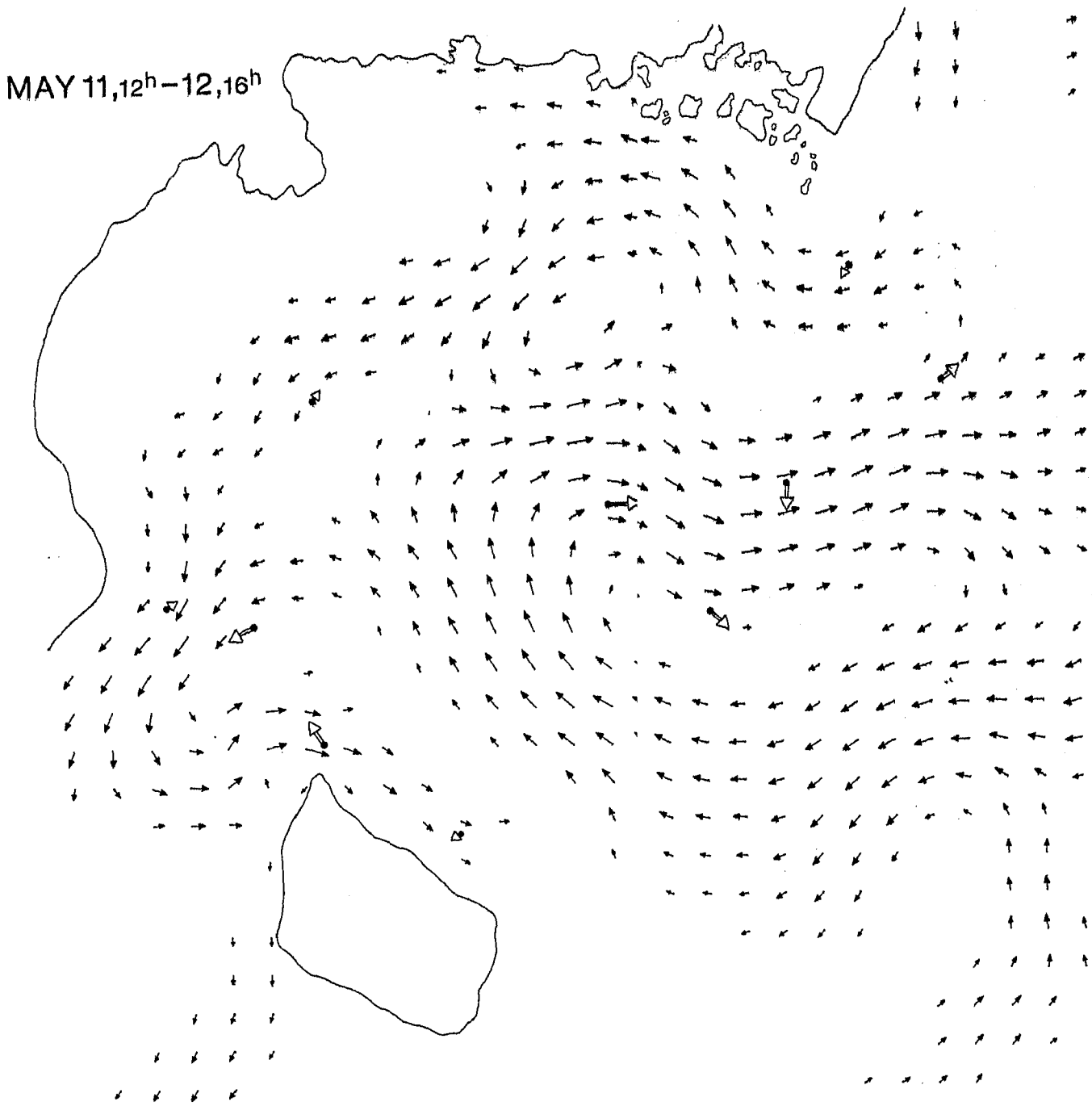

Fig.17f

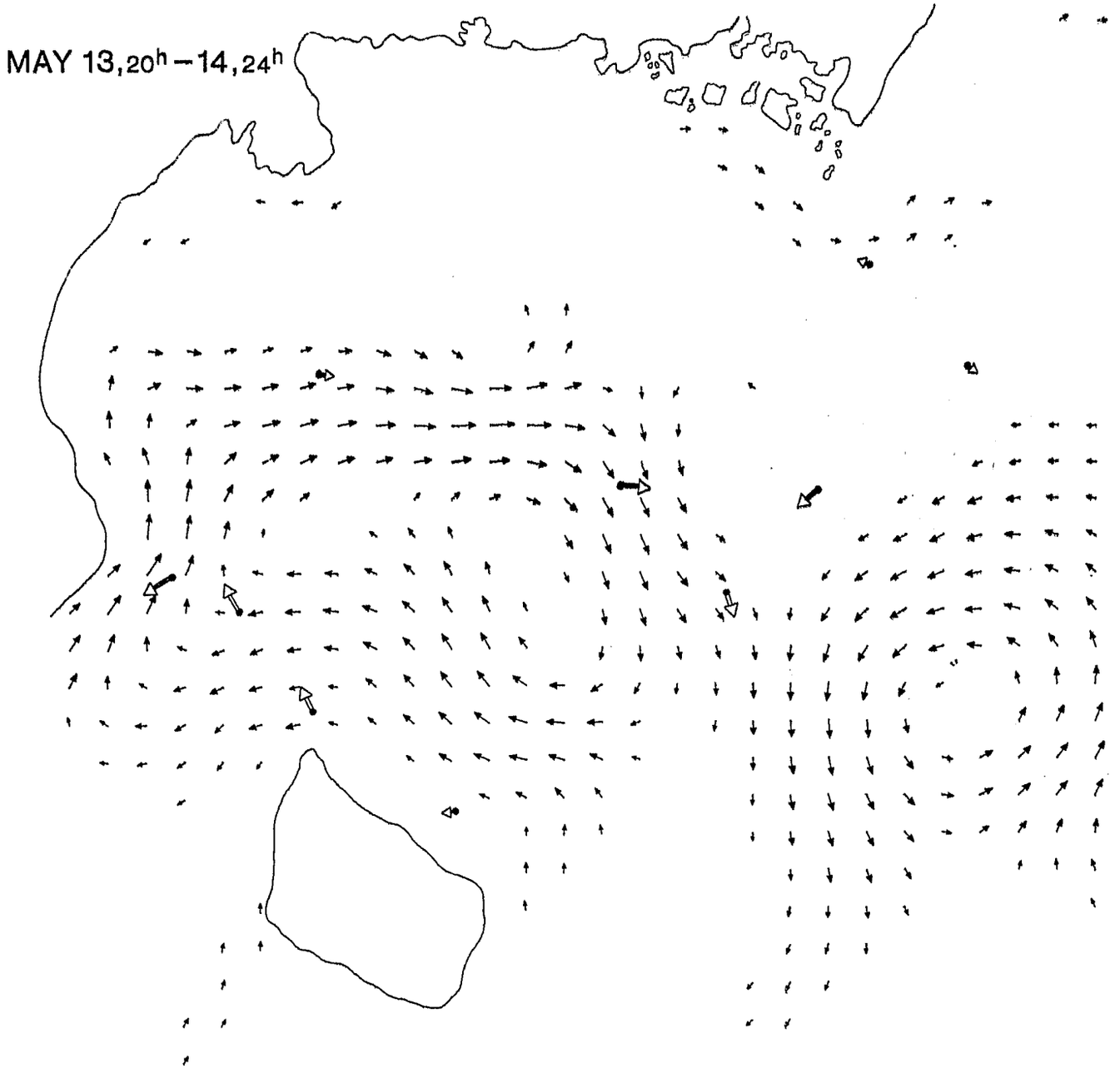

Fig.18

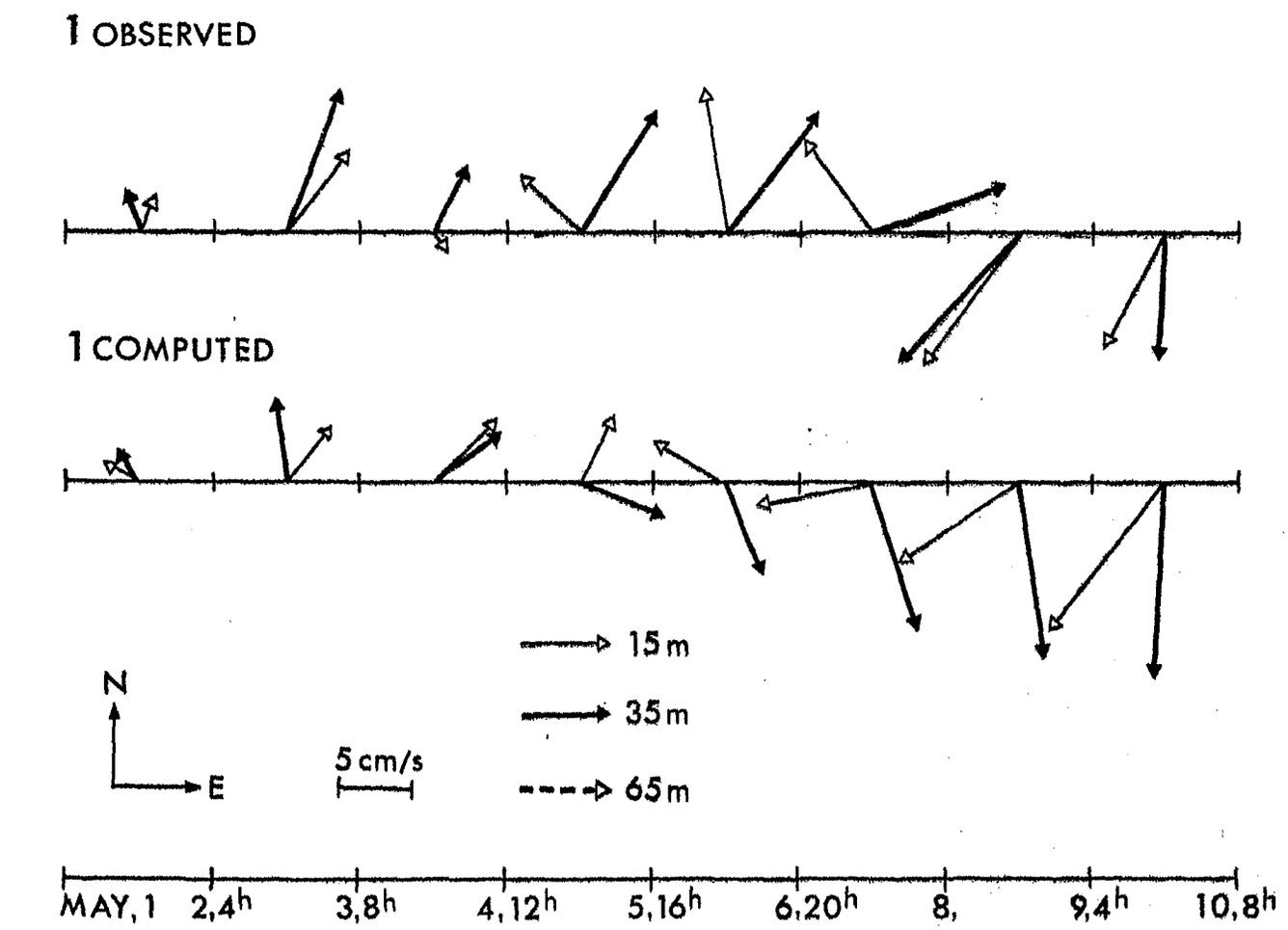
1 OBSERVED
1 COMPUTED
15 m
35 m
65 m
N
E
5 cm/s
MAY, 1
2,4h
3,8h
4,12h
5,16h
6,20h
8,
9,4h
10,8h

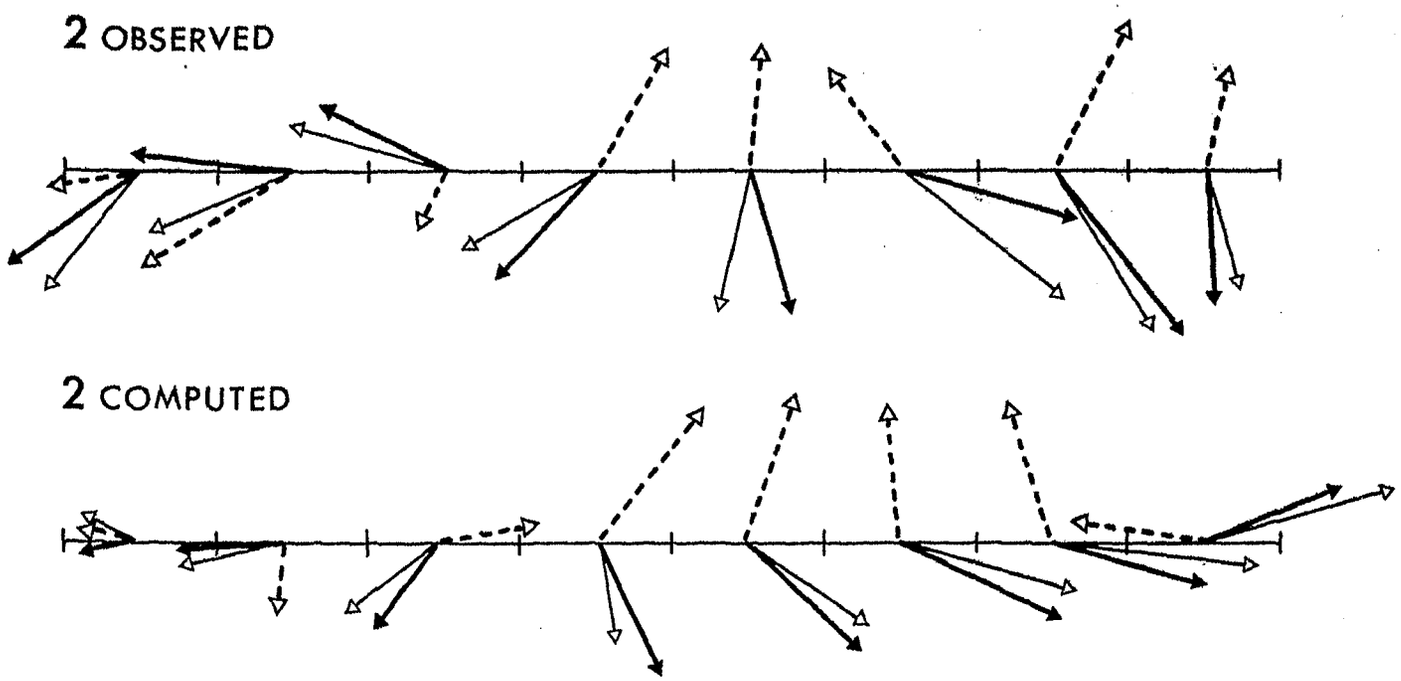
2 OBSERVED
2 COMPUTED

Fig.19

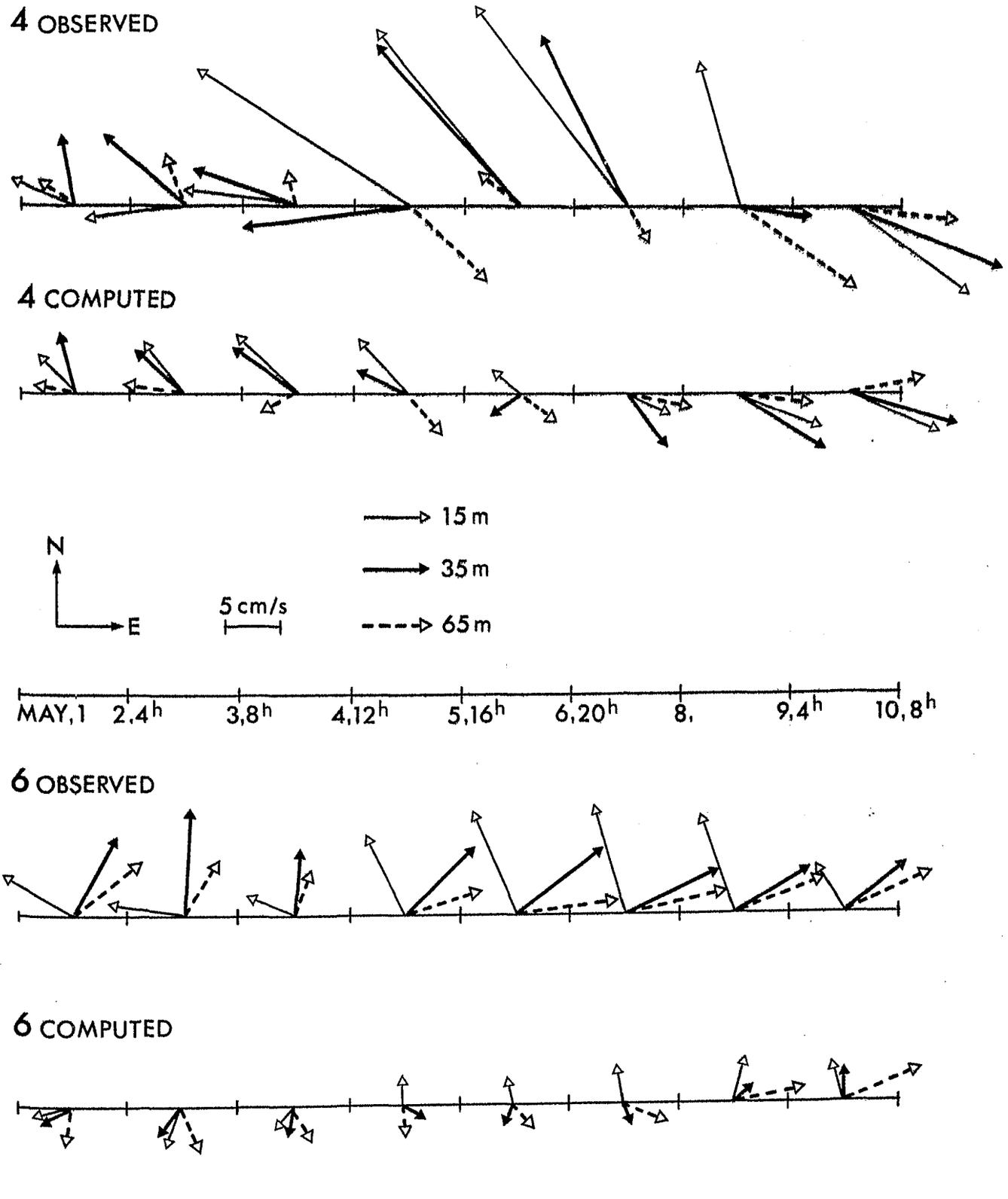
4 OBSERVED
4 COMPUTED
15 m
35 m
65 m
N
E
5 cm/s
MAY,1
2,4h
3,8h
4,12h
5,16h
6,20h
8,
9,4h
10,8h
6 OBSERVED
6 COMPUTED

Fig.20